C. elegans monitor energy status to trigger innate immune responses via AMPK pathway against bacterial pathogens

Donghai Peng (donghaipeng@mail.hzau.edu.cn)
Huazhong Agricultural University
Shouyong Ju
Huazhong Agricultural University
Hanqiao Chen
Huazhong Agricultural University
Shaoying Wang
Huazhong Agricultural University
Jian Lin
Huazhong Agricultural University
Raffi Aroian
University of Massachusetts Medical School
Ming Sun
Huazhong Agricultural University

Article

Keywords: surveillance systems, potassium leakage, AMP-activated protein kinase, innate immune responses, Caenorhabditis elegans, Bacillus thuringiensis

Posted Date: June 10th, 2021

DOI: https://doi.org/10.21203/rs.3.rs-590514/v1

Version of Record: A version of this preprint was published at Communications Biology on June 30th, 2022. See the published version at https://doi.org/10.1038/s42003-022-03589-1.

Abstract

Pathogen recognition and triggering pattern of host innate immune system is critical to understanding pathogen-host interaction. Cellular surveillance systems have been reported as an important strategy for the identification of microbial infection. In the present study, using *Bacillus thuringiensis-Caenorhabditis elegans* as a model, we found a new approach for surveillance systems to sense the pathogens. We report that *Bacillus thuringiensis* produced Cry5Ba, a classical PFTs, leading mitochondrial damage and energy imbalance by causing potassium ion leakage, instead of directly targeting mitochondria. Interestingly, *C. elegans* can monitor intracellular energy status through the mitochondrial surveillance system to triggered innate immune responses against pathogenic attack via AMP-activated protein kinase (AMPK). Obviously, it is common that pathogens produce toxins to cause potassium leakage. Our study indicate that the imbalance of energy status is a common result of pathogen infection.Besides. AMPK-dependent surveillance system can act as a new strategy for host to recognize and defense pathogens.

Introduction

Animals encounter diverse pathogens in natural environment, and they have evolved different defense responses against pathogens for survival. The principal challenge for the host is how to sense the pathogens and trigger defense responses. The innate immune system is a universal and evolutionarily ancient part of such host defense response [1].

It is generally accepted that hosts could discriminate pathogens from non-pathogenic bacteria in multiple ways. Firstly, the host can recognize microbe-associated molecular patterns (MAMPs) or endogenous danger-associated molecular patterns (DAMPs) by pattern-recognition receptors (PRRs) to induce immune signaling pathways [2]. This is also called pattern-triggered immunity (PTI), which is the most traditional way for hosts to identify pathogens. It is wellknow that MAMPs are highly conserved and common among microbes [3,4]. DAMPs are endogenous molecules secreted by damaged cells[5], which also implies that they are not the premier immune-activating factor. However, the PRR ligands are not unique to pathogenic bacteria, but also found in the non-pathogenic bacteria [6], making it hard to simply identify the pathogen in this way. Besides, the hosts could sense the existence or the damage caused by certain virulence factors to discriminates pathogens, which is called effector-triggered immunity (ETI) [7–9]. However, most of the ETI responses still depend on PPRs, while animals could still sense pathogens without activating PPRs [10]. Therefore, the PTI and ETI responses that relied on PPRs are not enough to explain pathogen recognition [11,12].

Recently, there is increasing studies concern about the host could indirectly detect pathogens through non-PPRs-related cellular surveillance responses. The host cellular surveillance systems could monitor the core cellular activities disorder caused by pathogens, triggering innate immune responses through non-PPRs-related ways. The integrity of nucleolus [13] or DNA [14], inhibits the transcription or translation

processes [12,15], and disruption of the mitochondrial protein folding environment [16,17] can be sensed by host cellular surveillance systems to initiate innate immune defenses. Consequently, the host cellular surveillance response is an important supplement strategy to PTI and ETI responses during pathogen recognition process. However, despite the continuous enrichment of the immune surveillance systems, the specific upstream signaling molecules and pathways representing the changes of cell homeostasis to induce the innate immune defenses remain largely unknown.

By far, the most classic reported cellular surveillance systems contain the ribosome, proteasome, and mitochondria [18]. Numbers of work showed that the mitochondria could be attacked by toxins produced from pathogens. Toxins from many bacterial pathogens like vacuolating toxin (VacA) [19], alpha-toxin[20], and leucocidin [21] can target and damage the mitochondria, leading to mitochondrial dysfunctional. Furthermore, *C. elegans* can activate mitochondrial UPR(UPR^{mt}) response by the transcription factor ATFS, which eventually engages the host innate immune defenses to defense pathogens [22,23]. These studies indicate that the mitochondrial surveillance system is an effective means for host to monitor pathogen infection.

The mitochondria are important biosynthetic and bioenergetic organelles and play a key role in cell homeostasis [24,25], Which can be perturbed by internal and external “stressors”[26]. Mitochondria can sense and respond to several kinds of stressors, such as environmental change, genetic mutation, endogenous molecules and even pathogens[27]. Several pathogen toxins can act as stressors to directly target mitochondrial or related proteins. However, mitochondria sense and respond to cell endogenous stressors caused by pathogens is remains to be studied

The *Caenorhabditis elegans* has been developed as a powerful model to understand innate immune responses. Many studies supported that *C. elegans* could monitor core cellular physiology activities to detect pathogen infections [12,15,18]. Moreover, there are no exact PPRs that have been unambiguously defined in *C. elegans* [28]. These facts make *C. elegans* an ideal model to study how surveillance systems sense pathogens through a no-PPRs pattern. *Bacillus thuringiensis* (Bt) is an obligate and opportunist pathogen of insects and worms, which produces insecticidal or nematicidal crystal protein during sporulation, and has been used as a leading bio-insecticide to control various pests and worms [29]. Here, we used a nematicidal Bt strain BMB171/Cry5Ba [30] and *C. elegans* as a model, to research the detailed mechanisms about how the cell surveillance systems sense pathogens and activate the innate immune responses. We showed that Bt infection causes a severely cellular energy imbalance by altered of AMP/ATP ratio. The energy imbalance is caused by the leakage of potassium resulted by Cry toxin and subsequent mitochondrial damage, instead of directly targeting mitochondria. While the Cry toxin-mediated mitochondrial damage will trigger the innate immune response via a cellular energy sensor AMPK in *C. elegans*. Our work revealed the mitochondrial surveillance systems can discriminate pathogens from the non-pathogenic bacteria by triggering innate immune responses via cell energy sensor AMPK during bacteria pathogen infection in *C. elegans*, which provided novel insights to understand host-pathogen interactions.

Results

B. thuringiensis **infection leads to cellular energy imbalance in** C. elegans

To investigate the intracellular physiological changes of *C. elegans* after pathogenic Bt infection, we conducted the *C. elegans* transcriptome analysis after infection by the nematicidal Bt strain BMB171/Cry5Ba, an acrystalliferous Bt mutant BMB171 transformed with toxin gene *cry5Ba* on the shuttle vector pHT304 [30]. As a control, we compared the transcriptome to a non-nematicidal Bt strain BMB171/pHT304, BMB171 transformed with the empty vector pHT304. Enrichment pathway analyses highlighted several pathways strongly affected by the infection of nematicidal Bt strain (Fig. 1A and Table S2). Interestingly, we found the energy metabolic related pathway was most strongly affected. This indicated that the regulators of the energy metabolic pathway may play important roles in host responses against Bt infection. To confirm this, we measured the concentrations of AMP and ATP by LC-MS [31] when wild-type *C. elegans* N2 fed with BMB171/Cry5Ba, the non-nematicidal control strain BMB171/pHT304 and the standard food strain *E. coli* OP50. The results showed that the AMP/ATP ratio had no significant difference after *C. elegans* N2 fed with BMB171/pHT304, but significantly increased after fed with BMB171/Cry5Ba, comparing with that of fed with *E. coli* OP50 (Fig. 1B). However, the AMP/ATP ratio showed no significant difference when the Cry5Ba-receptor mutant *bre-5(ye17)* worms were fed with either BMB171/Cry5Ba or BMB171/pHT304 (Fig. 1B). Next, we tested whether other nematicidal Bt can lead cell energy change, such as BMB171/Cry5Ca [30], BMB171/Cry6Aa [32], BMB171/Cry21Aa and non-nematicidal BMB171/Cry1Ac [33]. We found that nematicidal Bt strains can cause significant energy imbalance of *C. elegans* comparing with non-nematicidal Bt (Fig. S1). Taking together, we demonstrated that nematicidal Bt infection triggers a cellular energy imbalance of *C. elegans*, which was mainly attributed to the nematicidal toxins.

B. thuringiensis **infection leads to mitochondria damage**

Mitochondria produces most of the cell's ATP through oxidative phosphorylation and the tricarboxylic acid cycle, and plays a vital influence on cell metabolism [34]. Mitochondria are constantly in a state of fusion and division, which are essential for maintaining mitochondrial respiration and homeostasis, and even cell death [35,36]. It has been proved that PFT from pathogens can caused serious mitochondrial disruption in C. elegans[37]. Also, toxins from *Pseudomonas* pathogens can target mitochondria and lead to mitochondria fragmentation (MF) and it dysfunctional [16,17]. The MF phenomenon can result in bioenergetics defects, which cause cell energy imbalance [38]. To assess how nematicidal Bt causes cellular energy imbalance. We tested several physiological and biochemical aspects of mitochondrial damage including MF, mitochondrial membrane potential (ΔΨm), and mitochondrial DNA (mtDNA) content. We used the transgene worms SJ4143(*zcIs17*[P_{ges-1}::GFP^{mt}]) as MF reporter which stably expressed GFP in mitochondria matrix of intestinal cells to detect the mitochondrial morphology [39]. When worms fed with nematicidal Bt BMB171/Cry5Ba, 76.67% of worms showed MF (Fig. 2A and 2B). However, when worms were fed with non-nematicidal Bt strain BMB171/pHT304 or the standard food

strain *E. coli* OP50, the mitochondria morphologies of most worms kept tubular, only less than 15% of worms showed MF (Fig. 2A and 2B). These results showed that nematicidal Bt infection leads to MF. Next, we tested whether BMB171/Cry5Ba infection can cause changes in mitochondrial membrane potential (ΔΨm) and mitochondrial DNA (mtDNA) content. Using wild type N2 worms, we found BMB171/Cry5Ba infection can lead to a significant reduction in mitochondrial membrane potential (ΔΨm) and mtDNA content comparing with non-nematicidal Bt BMB171/pHT304 (Fig. 2C, 2D and S2).

When the Cry5Ba receptor related gene *bre-5* was silenced by RNA interference (RNAi) in transgene worms SJ4143(*zcIs17* [P_{ges-1}:: GFPmt]), only 12.22% of worms showed MF phenomenon after fed with BMB171/Cry5Ba (Fig. 2A and 2B), indicating that the Cry protein toxin Cry5Ba was the key factor that caused the MF phenomenon during Bt infection. However, when Cry5Ba-receptor null mutant *bre-5*(*ye17*) worms fed with BMB171/Cry5Ba in the same condition, the ΔΨm and mtDNA content were similar to *bre-5*(*ye17*) worms fed with BMB171/pHT304 (Fig. 2C-D). We conclude that Cry5Ba toxin is the key factor for Bt to manipulate host cell mitochondria and cause serious mitochondrial dysfunction.

Mdivi-1 is an efficient inhibitor to attenuates mitochondrial division by inhibiting the mitochondrial division dynamin, and it also suppresses mitochondrial outer membrane permeabilization [40]. To assess the relationship between cell energy imbalance and mitochondrial dysfunction after Bt infection, we checked whether mitochondrial division inhibitor mdivi-1 can recover mitochondria damage. We observed that mdivi-1 can effectively reduce Cry5B-mediated MF (Fig. 2A-B). Besides, our results showed that when wild type N2 worms were fed with BMB171/Cry5Ba adding mdivi-1, the AMP/ATP ratio was significantly reduced, the ratio of mtDNA/nDNA returned to normal levels (Fig. 2D-E). However, we found mdivi-1 cannot recover the reduction of mitochondrial membrane potential (Fig. 2C). In general, these results indicate that mitochondrial damage is responsible for the increase in intracellular AMP/ATP.

To assess whether other nematicidal Bt strains can cause MF phenomenon, we fed transgene worms SJ4143(z*cIs17* [P_{ges-1}:: GFP^{mt}]) with the other four nematicidal Bt BMB171/Cry5Ca, BMB171/Cry21Aa, BMB171/Cry6Aa, and non-nematicidal Bt BMB171/Cry1Ac. These former two strains produce Cry5-like three-domain (3D) group nematicidal Cry proteins Cry5Ca [30] and Cry21Aa [41], respectively. While BMB171/Cry6Aa produces a non-3D group nematicidal Cry toxin Cry6Aa [42]. The transgene worms SJ4143 fed with nematicidal BMB171/Cry5Ca, BMB171/Cry6Aa and BMB171/Cry21Aa exhibited the fragmented mitochondrial morphology (Fig. S3) with a range from 65.42–86.73% (Fig. S4). However, the worms fed with the and BMB171/Cry1Ac showed no significant MF phenomenon (Fig. S3 and Fig. S4). The results showed that the toxins from nematicidal Bt are capable of causing mitochondrial morphology damage in *C. elegans*.

B. thuringiensis -induced mitochondrial damage is the result of intracellular potassium leakage

The Cry5Ba toxin in Bt is a typical pore-forming toxin (PFT) which can form pores in the cell membrane, causing the unbalance in selectively permeable of the plasma membrane [43,44]. Mitochondria face various intracellular stressors, to explain the mechanism of Cry5Ba caused mitochondrial damage, we determine

the direct stressors of mitochondria in response to Cry5Ba. We first check whether Cry5Ba can target mitochondrial directly, our results showed Cry5Ba can be translocated into epithelial cells, but can't colocalize with mitochondria (Fig. 3A). In addition to target mitochondria directly, it had been proved PFTs can lead to severe ion dysregulation [45]. The osmotic imbalance caused by ion dysregulation has been demonstrated important to mitochondria [46]. Next, we assess the cellular Ca^{2+} and K^{+} levels after Bt infection. We found that Bt infection caused a significant decrease in potassium ion concentration, but not calcium ion. In a K^{+}-free environment, the leakage of potassium is more serious. When the potassium concentration increased, the leakage of potassium would be alleviated. But in *bre-5*(*ye17*) worms, potassium content did not change at any condition (Fig. 3A-3B and S5-S6). So we can conclude that during the Bt infection, Cry5Ba caused intracellular potassium leakage.

To verify our hypothesis that potassium leakage is the direct reason for mitochondrial damage. We detect the MF phenomenon during different potassium concentrations, we found during the Bt infection, the restoration of intracellular potassium can also reduce the MF phenotype, but serious potassium leakage caused a greater proportion of MF phenotypes (Fig. 3C). At the same time, the mitochondrial membrane potential could also return to normal level with potassium addition (Fig. 3D). As we found, the MF phenotype caused by Cry5Ba toxin is responsible to energy imbalance. More importantly, our results showed the restoration of potassium concentration can restore the content of AMP/ATP (Fig. 3E). Therefore, we concluded the leakage of potassium ions caused by Bt infection directly causes mitochondrial stress,which subsequently leads to mitochondrial damage and energy imbalance.

Cell energy imbalance mediated by mitochondria damage activates the AMP-activated protein kinase

The AMP-activated protein kinase (AMPK) is a sensor of energy status that maintains energy homeostasis and can be activated by a decrease in energy levels [47]. The synthesis and catabolism of ATP are largely regulated by AMPK [47]. AMPK is activated via phosphorylation of Thr172 on the α catalysis subunit (AAK-2 protein) [47]. It is well known that increasing of AMP/ATP proportion is the classical way to activate the AMPK [47]. We observed that *aak-2* was significantly up-regulated and the AMP/ATP ratios were significantly increased when worms are infected by nematicidal Bt (Fig. 1B and S7). Therefore, we speculated that nematicidal Bt infection may activate AMPK. To confirm this hypothesis, we performed western blotting to analyze the Thr172 phosphorylation of AAK-2 protein in worms. The results showed that the Thr172 of AAK-2 was phosphorylated when *C. elegans* fed with BMB171/Cry5Ba but not in the control strain BMB171/pHT304 treatment (Fig. 4A). What's more, the Thr172 of AAK-2 protein was not phosphorylated when Cry5Ba-receptor null mutant *bre-5*(*ye17*) worms were fed with BMB171/Cry5Ba under the same conditions (Fig. 4A). Inhibition of mitochondrial fragmentation using mdivi-1 could significantly suppress the Thr172 phosphorylation of AAK-2 (Fig. 4A). Besides, restore the leakage of potassium ions caused by Bt infection can also suppress the Thr172 phosphorylation of AAK-2 (Fig. 4B). These results demonstrated that the AMPK of worms is activated by nematicidal Bt infection via the phosphorylation of the core subunit AAK-2.

To assess the relationship between cell energy imbalance and the activating of AMPK after Bt infection, we knock down the *aak-2* transcription levels by RNAi in the mitochondria reporter worms SJ4143(zcIs17[P_{ges-1}:: GFP^{mt}]). Then, the non-RNAi and *aak-2* RNAi worms were fed with BMB171/Cry5Ba or BMB171/pHT304, respectively. The RNAi-*aak-2* worms also showed a high level of MF when worms fed with BMB171/Cry5Ba, most mitochondria keep tubular when worms fed with control strain BMB171/pHT304 (Fig. 4C-4D).

We also measured the concentrations of AMP and ATP when wild-type *C. elegans* N2 and RNAi-*aak-2* worms were fed with BMB171/Cry5Ba or BMB171/pHT304. The AMP/ATP ratio was significantly increased when RNAi-*aak-2* worms were treated with BMB171/Cry5Ba compared to BMB171/pHT304 (Fig. 4E). However, the increasing of AMP/ATP ratio was no significant difference when RNAi-*aak-2* and N2 worms were treated with BMB171/Cry5Ba (Fig. 4E). These results demonstrate that knockdown of the *aak-2* does not affect the level of MF and energy imbalance during Bt infection, and suggest that AMPK activation is a result rather than a cause of the above MF phenomenon. Thus, we concluded that Bt-mediated cell energy imbalance activates the AMPK in *C. elegans.*

AMPK activation is involved in C. elegans **defense responses against Bt infection**

Several previous studies reported that AMPK defends against low glucose levels, dietary deprivation, paraquat, physical stress and pathogens [48–50]. Therefore, we asked whether AMPK activation might be involved in defense against Bt infection. There are three subunits for the AMPK complexes, including a catalytic subunit (α), and two regulatory subunits (β and γ). To confirm this hypothesis, we tested the sensitivity of these four AMPK null alleles mutants and the wild type N2 worms exposed to BMB171/Cry5Ba, including *aak-1*(*tm1944*) (subunit α1 of AMPK), *aak-2*(*ok524*) (subunit α2 of AMPK), *aakb-1*(*tm2658*) (subunit β1 of AMPK), and *aakg-4*(*tm5269*) (subunit γ1 of AMPK). Compared to the wild type N2 worms, only *aak-2*(*ok524*) mutant worms showed more increased sensitivity to BMB171/Cry5Ba infection (Fig. 5A and Fig. 5B). Survival assays confirmed that the *aak-2*(*ok524*) mutant worms are more sensitive to BMB171/Cry5Ba infection (Fig. 5C).

To further confirm the importance of AMPK catalysis subunit α2 (AAK-2 protein) in defense to BMB171/Cry5Ba infection, we tested the sensitivity of null allele of *aak-2* mutant worms, *aak-2*(*gt33*), feeding on BMB171/Cry5Ba. We found that *aak-2*(*gt33*) is also more sensitive to BMB171/Cry5Ba than wild type N2 (Fig. S8). A similar phenotype was observed in *aak-2* RNAi worms (Fig. S9).

We next asked whether the AMPK subunit α2 knockout phenotype is specific for Bt infection. The sensitivity of the wild type N2 and *aak-2*(*ok524*) mutant worms were analyzed to the heavy metal copper sulfate and oxidative stress (hydrogen peroxide). Our results showed that it is no significant difference in these treatments between the wild type N2 and the mutant *aak-2*(*ok524*) worms (*t*-test, $p > 0.05$) (Fig. S10A and S10B).

In addition, we activated AMPK using 5-Aminoimidazole-4-carboxamide 1-ß-D-ribofuranoside (AICAR), a typical activator stimulating AAK-2 kinase activity of AMPK via phosphorylation of Thr172 on α catalysis

subunit (AAK-2 protein) [51]. Western blotting results showed that the AMPK is activated by 50 μM of AICAR via AAK-2 Thr172 phosphorylation (Fig. 3A). We then compared the sensitivity of the AICAR-treated with non-treated N2 worms to BMB171/Cry5Ba infection by survival assays and growth assay, respectively. The results showed that the AICAR-activating worms showed more significant resistance to BMB171/Cry5Ba infection comparing with the no-activating N2 worms (Fig. 4D and 4E). However, compared with the wild type N2 worms, the resistance to BMB171/Cry5Ba infection was not significantly different for *aak-2* mutant either in AICAR-activating or no-activating conditions (Fig. 4D and 4E). Taking together, our results demonstrated that AMPK plays an important role in *C. elegans* defense against BMB171/Cry5Ba.

AMPK activity in the intestine is required for C. elegans resistance to Bt infection

To independently confirm the importance of AAK-2 in defense to BMB171/Cry5Ba infection, we constructed the transgenic strain *aak-2*(*ok524*) (P_{aak-2}::*aak-2*), which expresses the *aak-2* under the control of its native promoter P_{aak-2} to rescue the *aak-2* function under the background of mutant *aak-2*(*ok524*) worms. The growth assay and survival assay results showed that *aak-2* expression driven by its own promoter P_{aak-2} can completely alleviate the hypersensitivity of *aak-2*(*ok524*) mutant to BMB171/Cry5Ba infection (Fig. 6A and 6B), supporting that AAK-2 is independently important for worms to defense BMB171/Cry5Ba infection.

C. elegans apparently lacks professional immune cells, but can rely on epithelial cells for immune defenses [52]. Cry5Ba can attack the intestine of worms and forming pores in the membrane of the intestine cell [53,54]. We therefore hypothesized intestinal-specific activity of AMPK regulates immune responses to Bt infection immediately. We drove the *aak-2* expression under different tissue-specific promoters, including the intestine-specific promoter P_{vha-6} [55], the muscle-specific promoter P_{myo-3} [56], and the neuron-specific promoter P_{rab-3} [57]. We found that only *aak-2* expression under the intestine-specific promoter P_{vha-6} alleviated the hypersensitivity of *aak-2*(*ok524*) mutant to BMB171/Cry5Ba infection (Fig. 6C and 6D). In contrast, there were no significant difference in hypersensitivity to Bt infection among the *aak-2*(*ok524*) mutant and the muscle-specific P_{myo-3} or neuron-specific P_{rab-3} rescued worms (Fig. 6C and 6D). Also, we knocked down the *aak-2* gene by RNAi in the intestine, muscle, and epidermis of worms, respectively. Only the intestine-specific knock-down of *aak-2* made the worms more sensitive to BMB171/Cry5Ba infection (Fig. 6E). In contrast, epidermal-specific or muscular-specific *aak-2* RNAi worms did not (Fig. S11A and S11B). These results suggest that the intestine serves as the first line of AMPK-mediated defense against BMB171/Cry5Ba attack.

AMPK activation triggers DAF-16 dependent innate immune singling pathway during Bt infection

AMPK pathway is evolutionarily conserved from *C. elegans* to mammals and regulates many downstream pathways [58]. Here, AMPK has been shown to play a role in the defense of Bt infection in *C. elegans*. However, the AMPK downstream genes or pathways involved in the defense against Bt infection

in *C. elegans* were not clear. It was reported that AAK-2 is capable of modulating the phosphorylation of the FOXO family transcription factor DAF-16, activating the DAF-16-dependent transcription when worms suffering from dietary restriction [59]. DAF-16 can regulate many genes involved in metabolism, immune responses against several pathogens, and longevity of *C. elegans* [60,61]. Moreover, the DAF-16 was also triggered by nematicidal Bt infection [62], and functioned as an important modulator in defense against nematicidal PFTs in *C. elegans* [63]. Therefore, we speculated that AMPK may regulate the DAF-16-dependent signaling pathway in defense against Bt infection. To confirm this hypothesis, we compared previously identified DAF-16 target genes [60] with our RNA-Seq data. We found 60 of the genes up-regulated by Bt infection are also the targets of DAF-16 (Fig. 7A, Table S3 and S4) (*t*-test, $p < 0.001$). To verify this analysis, we selected 8 typical genes from these genes and determined their transcription by qPCR. The transcription of these 8 genes was significantly up-regulated after Bt infection in wild type N2 worms. Moreover, RNAi of *daf-16* significantly suppressed the up-regulation of these genes induced by Bt infection (Fig. 7B), and RNAi of *aak-2* also suppressed most gene upregulation, supported that these DAF-16-dependent genes are also regulated by AAK-2 during Bt infection.

Under standard growth conditions, DAF-16 is distributed predominately throughout the cytoplasm of all tissues. When activated, DAF-16 will be phosphorylated and translocated from cytoplasmic to the nucleus, then binds to the promoter region and activates the expression of target genes [60]. Therefore, we monitored the cellular translocation of DAF-16 using transgenic worms TJ356(*Isdaf-16*:: *gfp*) as a reporter, which expresses functional DAF-16:: GFP fusion protein. Our results showed after BMB171/Cry5Ba infection, most of the DAF-16:: GFP was translocated from the cytoplasm to the nucleus in the intestine, especially the front and middle parts of the intestines (Fig. 7C and 7D). In contrast, the control strain BMB171/pHT304 failed to cause DAF-16 transfer to the nucleus at the same conditions (Fig. 7C, 7D and Fig. S12). These results demonstrated that nematicidal Bt infection can activate the DAF-16 nuclear translocation in wild-type worms.

To test whether the AMPK activity is required for the activation of DAF-16 during Bt infection, we monitored the cellular translocation of DAF-16 when the *aak-2* gene was silenced by RNAi in the reporter worm TJ356 (*Isdaf-16*::*gfp*). The observations showed that the DAF-16 nuclear translocation induced by Bt is significantly diminished by RNAi *aak-2* gene (Fig. 6C and 6D). To test whether DAF-16 activation can trigger the transcription of the downstream immune-related effectors, we tested the expression of *sod-3*, a well-known direct target of DAF-16 during Bt infection [64]; *sod-3* gene is also one of the most significant up-regulated genes in Bt-infected worms (Table S3 and S4). We observed the expression of *sod-3* using transgenic worm CF1553(*muIs84*(sod-3::GFP)) [64]. When the SOD-3::GFP reporter worms were exposed to BMB171/Cry5Ba, the expression of *sod-3* was significantly up-regulated compared to BMB171/pHT-304. Meanwhile, the induction of *sod-3* by BMB171/Cry5Ba infection was significantly inhibited when either *daf-16* or *aak-2* gene was silenced in the strain CF1553(*muIs84*(sod-3::GFP) (Fig. 7E and 7F). Additionally, the *aak-2* deletion also significantly suppressed the up-regulation of the above selected 8 immune-related genes induced by Bt infection (Fig. 7B). Taking together, we concluded that the AMPK triggers the DAF-16-dependent innate immune pathway during Bt infection.

Discussion

Pathogen recognition and triggering the host innate immune system is critical to understanding pathogen-host interaction [65]. It is generally accepted that the microbial infection can be recognized by host PTI and ETI patterns which are related to PRR. However, due to the limitations of PRR ligands, these conserve innate immune pathways are not enough to distinguish pathogens from some probiotic or symbiotic bacteria. But the ETI hypothesis is an important supplement to PTI and proposes that the host responds to pathogens by monitoring bacterial virulence factors [9,66]. Moreover, cellular surveillance systems, including the ribosome, proteasome, and mitochondria, monitor core cellular physiology activities were considered as a novel pattern for hosts to distinguish pathogens from other microorganisms [18]. However, how host cells using these systems to sense pathogens are unclear. There are several ways for the host to recognize the pathogens by monitoring core cell processes, including the DNA damage [14], the inhibition of translation [15], and the UPR^{mt} during the mitochondrial damage state [67], etc. Here, we revealed that the leakage of potassium caused by pathogens leads to mitochondrial stress, and then host cells could sense pathogens via mitochondria mediated intracellular energy imbalance. Therefore, our work provides a novel insight for the host cell to detect pathogens through cellular surveillance systems.

Previous works have shown several pathogens could attack and disrupt host mitochondria [16,68,69]. In our study, damage to the mitochondria was also detected when worms were infected by nematicidal Bt, including MF, a decrease in mitochondrial membrane potential, and the changes in mtDNA content (Fig. 2). The damages to the mitochondria during Bt infection were mainly caused by its key virulent factor, Cry5Ba toxin (Fig. 2 and S2). Although Cry5Ba could be translocated into epithelial cells, we did not find evidence of colocalization with mitochondria (Fig. 3A), indicating Cry5Ba may lead to mitochondrial dysfunction indirectly. Next, we confirmed that the leakage of intracellular potassium caused by Cry5Ba led to the mitochondrial damage directly (Fig. 3B). This model is different from extensively studied toxins produced by *P. aeruginosa* [16] or *L. monocytogenes* [68].

Cellular energy imbalance is an important sign of mitochondrial disorder. In fact, several PFTs such as streptolysin O, *Vibrio cholera* cytolysin, *Staphylococcus aureus* α-toxin, and *Escherichia coli* hemolysin A, could also cause a decrease in intracellular ATP levels in a non-virally transformed human keratinocyte cell line [70]. Our results showed that Bt infection could cause a Cry-dependent cellular energy imbalance, which was widespread among nematicidal Bt infection (Fig. 1B, Fig. S3 and Fig. S4). Both mitochondrial dysfunction and cytosolic energy imbalances were restored in a Cry5Ba receptor mutant (*bre-5*), indicating toxin from nematicidal Bt is critical for these phenomena. Conversely, the mitochondrial division inhibitor mdivi-1, which can inhibit mitochondrial fragmentation but not the function of PFTs, can protect cells from AMP/ATP ratio imbalances. Besides, the recovery of intracellular potassium concentration caused by Cry5Ba can also alleviate energy imbalances (Fig. 3C-3D). Thus, the pores caused by the toxin are the primal reason for the changes in intracellular energy, and potassium leakage is the direct reason.

Previous research indicated that cytosolic energy imbalance and calcium content are the important AMPK triggering patterns [71]. We found Bt infection did not induce the increase of cytoplasm calcium level of worms (Fig. S6). Rather, nematicidal Bt infection led to mitochondria damage, which then gave rise to the dramatic increase of AMP/ATP ratio and AMPK activation via phosphorylation of α-catalysis subunit protein AAK-2 (Fig. 2A). Next, we found that the inhibition of mitochondrial fragmentation recovered the mtDNA content, restored abnormal AMP/ATP content, and inhibited the activation of AMPK (Fig. 2). These data suggest that MF was the reason why the AMP/ATP content changed when the mitochondria had been damaged. We also found that Bt infection led to a decrease in mitochondrial membrane potential, which is well known to be a consequence of mitochondrial ATP [72]. Besides, our work revealed that restoring potassium can not only restore mitochondrial damage, but also restore energy imbalance and AMPK activation. Together, our work revealed Bt infection increased the rate of AMP/ATP and cytosolic energy imbalance, which ultimately triggers AMPK via AAK-2 phosphorylation.

Accumulating evidence suggests that AMPK is not only a crucial evolutionarily conserved cellular energy sensor but also plays an important role in host-pathogen interactions [49]. Our work proved the activation of AMPK is helpful for *C. elegans* to defense nematicidal Bt (Fig. 5). What's more, the AMPK activity in intestinal cells is particularly important for *C. elegans* against nematicidal Bt (Fig. 6). As we know, due to the lack of professional immune cells, the *C. elegans* intestine is considered to be the first line to identify and defense against pathogens[73]. Therefore, we can infer that the host cell monitors the energy imbalance caused by pathogens through mitochondria, and then activate a series of responses against pathogens. Our work highlighted the importance of the connection between the cellular mitochondria surveillance systems and AMPK through energy changes during pathogen infection.

Additionally, how mitochondria disorder triggering downstream innate immunity signaling is largely unknown yet. Accumulating evidences showed that AMPK is also an important trigger of FOXO family transcription factors. DAF-16 regulated by the AMPK pathway is related to defense response against nutrition deprivation and functions to extend lifespan [48,59]. Here, we found that the AMPK activation mediated by mitochondrial damage regulates the DAF-16 to increase the transcription of certain DAF-16-dependent innate immune effectors, which helps *C. elegans* defend against pathogen infection (Fig. 7). The different sensitivity in several worms against Bt infection indicating that the AMPK is not the only way to activation of DAF-16 (Fig. S13A). At the same time, AMPK may regulate other DAF-16-independent innate immune pathways during Bt infection. MAPK pathway is also reported to be a downstream component of the AMPK signaling pathway in mammal cells [74]. The xenophagy for defense against pathogens infection was observably activated by the AMPK-dependent p38 MAPK pathway [75,76]. Under the infection of nematicidal Bt, the up-regulated of 3 typical genes of p38 MAPK pathway (*pmk-1, tir-1* and *sek-1*) together with the activation of PMK-1 demonstrated that AMPK also triggered the p38-MAPK innate immune pathways apart from DAF-16 during Bt infection (Fig. S13B and S13C).

In conclusion, our works demonstrated that host cells can directly sense mitochondrial-mediated intracellular energy imbalance to monitor pathogens, and activate downstream innate immune responses

to defense pathogens through activation of the AMPK pathway. As modeled in Fig. 8, nematicidal Bt infection in *C. elegans* caused potassium leakage, leading to the mitochondria damage and the energy imbalance of intestinal epithelial cells, the latter of which subsequently triggered AMPK *via* phosphorylation of AAK-2. Then, the AMPK modulates DAF-16-dependent and p38-MAPK-dependent innate immune pathway to defend against nematicidal Bt infection. These findings revealed that AMPK senses the changing of cellular energy imbalance and triggers the innate immune responses during pathogen infection. Consider that the mitochondria surveillance systems and AMPK are conserved components from worms to mammals, our study suggests that disrupting mitochondrial homeostasis to activate the immune system through AMPK-dependent pathways may widely existing in animals, which may provide new strategies for immunotherapy of multiple diseases.

Materials And Method

Caenorhabditis elegans **and bacterial strains.** *Caenorhabditis elegans* strains used in this work were kindly provided by the *Caenorhabditis* Genetics Center (CGC) or the National Bioresource Project (NBRP) and listed in Table S1. All *C. elegans* strains were maintained on nematode growth media (NGM, 0.3% NaCl, 0.25% tryptone, and 1.5% agar) using *E. coli* OP50 as food under standard conditions [77]. The bacterial strains and plasmids used in this study are also listed in Table S1. All *Escherichia coli* and Bt strains were grown on Luria-Bertani (LB) medium supplemented with the appropriate antibiotics at 37°C or 28°C, for *E. coli* or Bt, respectively. BMB171/Cry5Ba, BMB171/Cry5Ca, BMB171/Cry21Aa, BMB171/Cry6Aa and BMB171/Cry1Ac used in this work is the recombinant Bt that is the acrystalliferous Bt mutant BMB171 transformed with toxin gene *cry5Ba*, *cry21Aa*, *cry6Aa* and *cry1Ac* on shuttle vector pHT304 [78,79], respectively. BMB171/pHT304 used in this work is the acrystalliferous Bt mutant BMB171 transformed with an empty shuttle vector pHT304.

Construction of gene aak-2 **rescued worms.** A 2.1 kb fragment of the intestine-specific *vha-6* promoter (P_{vha-6}), a 2.5 kb fragment of the muscle-specific *myo-3* promoter (P_{myo-3}), a 1.3 Kb fragment of the neuron-specific *rab-3* promoter fragment (P_{rab-3}) and a 3.0 Kb fragment of *aak-2* promoter fragment (P_{aak-2}) were generated by PCR from total DNA of *C. elegans*, then inserted into pPD49.26 to gain 4 recombinant plasmids of pPD49.26-P. A full-length a 1.8 Kb of the *aak-2* cDNA and a 1.6Kb of the 3-UTR of *aak-2* was generated by overlap PCR and inserted into pPD49.26-P at the downstream of the promoters respectively. The recombinant plasmids which contained gene *aak-2* with the tissue-specific promoters, P_{aak-2}::*aak-2*, P_{vha-6}::*aak-2*, P_{myo-3}::*aak-2* and P_{rab-3}::*aak-2*, were injected into the gonads of *aak-2(ok524)* worms to generate independent transgenic lines by standard germline transformation techniques [80]. All of the 4 fusion genes were injected at concentrations ranging 100 ng/μl with P_{lin-44}::GFP at 100 ng/μl as a co-injection marker.

RNA interference. RNAi *E. coli* strains containing targeting genes were originally delivered from the Ahringer RNAi library [81] and were kindly provided by Professor Zhenxing Wu, Huazhong University of

Science and Technology. RNAi feeding experiments were performed as described before [81] on synchronized L1 larvae at 20°C for 40 h.

Quantitative real-time RT-PCR analysis. Total RNA isolated using Trizol reagent (Invitrogen) was reversely transcribed with random primers using Superscript II reverse transcriptase (Invitrogen) according to the manufacturer's protocol. Real-time PCR analysis was performed with Life Technologies ViiA™ 7 Real-Time PCR system (Life Technologies, USA) using Power SYBR Green PCR Master Mix (Life Technologies, USA). The gene *tba-1* was used as an internal reference [82]. The primers used for PCR are listed in Table S1. The experiments were conducted in triplicate, and the results were expressed as $2^{-\triangle\triangle Ct}$.

Nucleotide measurements. The AMP, ADP and ATP were extracted by the adapting perchloric acid method [83], 300–400 worms were washed with ice-cold M9 buffer, and resuspended in 20 μl of M9 buffer, then added 40μL of ice-cold 8% (v/v) $HClO_4$ on ice. The worms were then homogenized in liquid nitrogen, and the homogenates were disrupted using ultrasonic vibrations and neutralized with 1 N KOH. Next, the suspension was centrifuged (10,000g for 3min at 4°C), and the supernatant was passed through a 0.2 μm filter (Nanosep). The concentration of AMP, ADP and ATP were detected using the LC-MS (Agilent Technologies, 1260–6540). The operation of detection is based on the published method[84,85].

Analyses of mitochondrial morphology. SJ4143(*zcIs17*[P_{ges-1}::GFP^{mt}]) worms can stably express GFP in mitochondria matrix of intestinal cells. It can be used as a reporter for mitochondrial morphology. The worms were synchronized according to the method described before [39]. Then the worms were treated according to the liquid assay. Washed worms were collected to be photographed by Olympus BX63 with excitation at 488 nm and emission at 525 nm. At least three repeats were performed for each condition with and at least 50 animals photographed per treatment.

Measurement mitochondrial membrane potential (ΔΨm). Tetramethyl rhodamine ethyl ester (TMRE) ((MCE, # 115532-52-0)) is a lipophilic cation to detect the membrane potential (ΔΨm) of the mitochondrial [86]. Synchronized N2 worms were treated according to the liquid assay. After treated by respective bacteria and compounds, worms were resuspended in M9 containing 8μM TMRE. After two hours' treatment, worms were washed with M9 for 3 times to remove dye thoroughly. Worms were photographed using Olympus BX63 epifluorescence microscope at 10 × magnification with excitation at 550 nm and emission at 575 nm. At least three repeats were performed for each condition and at least 20 animals were measured per treatment. The average optical density of each worm was measured using Image Pro Plus v6.0.

Mitochondrial DNA (mtDNA) quantification assay. MtDNA damage was assessed using Real Time-qPCR according to the published method. [87,88] The pair of primers (Forward: GTTTATGCTGCTGTAGCGTG, Reverse: CTGTTAAAGCAAGTGGACGAG) were used to normalize the mitochondrial genome. The results were normalized to genomic DNA using primer pairs specific for *ama-1*(Forward: TGGAACTCTGGAGTCACACC, Reverse: CATCCTCCTTCATTGAACGG). Synchronized worms were treated and collected as described above. Collecting worms were homogenized in liquid nitrogen and lysed in a

standard buffer containing proteinase K for 1 hour at 65℃. qPCR procedure was implemented as described above.

Calcium and Potassium imaging. Fluo-4 AM (Molecular Probes) and ION Potassium Green-2 AM (APG-2 AM, Abcam) are used to detect the concentration of $Ca^{2+}$and K^{+} respectively, according to the published methods[89,90]. The treated *C. elegans* were loaded with 100 μM Fluo-4 AM for 1 h in M9 buffer. *C. elegans* were washed more than 3 times and then photographed by Olympus BX63 epifluorescence microscope. For K^{+}, treated *C. elegans* were labeled in 5μM APG-2 AM in each buffer of different potassium concentrations for 1 hour. The labeled *C. elegans* need to be cultured in the corresponding buffer added OP50 for 1 hour to remove the free dye in the intestine. The washed *C. elegans* were photographed under the same conditions. The excitation and emission wavelengths of Fluo-4 AM were 489 nm and 508 nm. For APG-2 AM, they are 526nm and 550nm, respectively. At least three repeats were performed for each condition and at least 20 animals were measured per treatment. The average optical density of each worm was measured using Image Pro Plus v6.0.

Bt infection assay. The Bt infection assays were based on the published protocol [91]. which contains two different procedures.The plate assays: Bt strains were grown in LB medium containing 50μg/ml spectinomycin at 28°C overnight and seeded 400μl to fresh NGM plate. Then these plates were placed at 28°C for 3 days. Synchronized nematodes were grown to L4 stage in NGM plate containing OP50. Nematodes were then washed off and cleaned by M9 buffer. 2000–3000 worms were added to the Bt plate and treated at 25°C for 4-6h. The liquid assay: Synchronized L1 worms were grown to L4 stage on OP50 plate at 20°C. Then 300–500 worms were added on a 24-well plate (total volume 50 μl) which containing 400μl M9 buffer. Then add different mixture of crystal toxins and spores to each well (total volume 50ul). The plates were placed at 25°C for 4-6h.

The growth assays. The L1 growth assays were carried out in different doses of the mixture of crystal Cry5Ba and spores as described before [91], *E. coli* OP50 was added at an optical density of 0.2–0.25 OD_{600} and 20–30 synchronized L1 larvae were used per well. After 3 days at 20°C, photographed at least 60 worms in different doses on a microscope, and calculated the average area for each condition using the software NIH Image J 1.33, normalized the average area at each toxin concentration to the average area of the no toxin control. The size of the worms in the absence of toxin was set at 100%. Each experiment was independently replicated at least three times.

The survival assays. The survival assays were conducted in different doses of the mixture of crystal Cry5Ba and spores as described before [91]. *C. elegans* N2 and these mutant worms were exposed to the mixture of crystal Cry5Ba and spores in S media in 96-well plates to quantitatively score the survival. Concentrations of each toxin were set-up in triplicate for each assay with approximately 20–30 synchronized L4 worms per well. The determination of whether worms were alive is according to the worms' movement. The crawling worms were marked as alive. Non-crawling worms should be gently touched with a platinum pick to observe their movement. The survival rate of each well was scored after incubating at 20°C for 6 days. Each experiment was independently replicated at least three times.

Lifespan assays. The life span assay was performed at 20°C on NGM plates. Each bacterium must be fully spread on the NGM plate to prevent worms from avoiding or escaping the bacteria lawn. Approximately 60 L4-stage worms were incubated on NGM plate seeded with OP50 or other pathogens. Every plate contained 0.05 mg/ml of 5-fluorodeoxyuridine (FUDR) to prevent eggs from hatching. Five plates were tested for each strain in each experiment. Each experiment was independently replicated at least three times. The determination of whether worms were alive was as described for the survival assay of *C. elegans*. The surviving worms on each plate were counted at 20 °C every 12 h. Statistical analyses were assessed by Kaplan-Meier survival analysis followed by a log rank test. Statistical significance was assessed by Kaplan-Meier survival analysis followed by a log rank test.

$CuSO_4$ and H_2O_2 assay. $CuSO_4$ and H_2O_2 assay were conducted as previously described [92]. The survival assays were conducted in serial doses of $CuSO_4$ or H_2O_2, 20–30 L4 synchronized worms were used per well in 48-well plates, *E. coli* OP50 at an optical density OD600 was 0.2–0.25. The survival rate of each well was determined after 6 days of $CuSO_4$ or 4 hours of H_2O_2 exposure at 20°C.

Cry5Ba localization assay. The L4-staged transgenic worms RT311[P_{vha-6}::*GFP::RAB-11*], which was an apical recycling endosome reporter [93] and SJ4143(*zcIs17* [P_{ges-1}::GFP^{mt}]), which was chosen as mitochondria reporter worm and can stably expressed GFP in mitochondria matrix of intestinal cells[39], were fed with rhodamine-labeled crystal protein Cry5Ba (a pore-forming toxin produced by Bt) 4 hours, then these worms were placed on 2% agarose pads, the signals of rhodamine-labeled and GFP-labelled were observed using the using confocal microscope at 100×magnification. At least 2–3 independent biological repeats were carried out for each experiment.

DAF-16 nuclear localization assay. After 2 h of treatment with Bt, the synchronized L4 TJ356 worms (transgenic animals expressing DAF-16::GFP) were immediately placed in M9 buffer and onto microscope slides. GFP localization was observed using a fluorescent microscope (Olympus BX31, Japan) at 40×magnification. DAF-16 localization was categorized as cytosolic localization, intermediate localization and nuclear localization. The number of worms with each level of nuclear translocation was counted. The worms were exposed to non-nematicidal Bt BMB171/pH304 were used as negative controls; while the worms were exposed to heat shock for the same periods at 30°C were used as a positive control. *P* values were calculated using SPSS ver13.0 (SPSS, Chicago, IL).

Western Blotting Analysis. After feeding Nematicidal *Bt* or Non-nematicidal Bt, *C. elegans* N2 and different mutants were washed three times with ice-cold M9 buffer and were homogenized in liquid nitrogen. Then homogenates were harvested in lysis buffer (50 mM HEPES, 150 mM NaCl, 10% glycerol, 1% Triton X-100, 1.5 mM MgCl2, and 1 mM EGTA) with protein inhibitors (0.2mM Na_3VO_4, 1mM NaF). The lysate samples were subjected to SDS-PAGE using 10% (wt/vol) polyacrylamide gels and transferred to PVDF membranes (Life technologies). The trans blotted membrane was washed three times with PBS containing 0.05% Tween 20 (PBST). After blocking with PBST containing 5% BSA, the membrane was probed with the primary antibody (Phospho-AMPKα(Thr172) Rabbit mAb, Cell Signaling, # 2535, or β-

actin Antibody, Proteintech, # 66009) and washed three times. The membrane was then probed with HRP-coupled secondary antibody and washed. Finally, the membranes were exposed using a chemiluminescent substrate (SuperSignal West Pico, Thermo Scientific).

RNA-sequencing and transcriptome analysis. Total RNA was isolated using Trizol reagent (Invitrogen, USA) according to the manufacturer's protocol. Total RNA concentrations and integrity were measured with NanoDrop 2000C spectrophotometer (Thermo Scientific, USA). The mRNA of each sample was purified using poly-dT oligo attached magnetic beads, and then fragmented (approximately 200 bp) at an increased temperature. The first strand cDNA was synthesized with random oligonucleotides and SuperScript II (Invitrogen, USA). The second-strand cDNA was synthesized by DNA polymerase I and RNase H. The second-strand cDNA was purified with Vahtstm DNA Clean Beads. Ends were repaired and 3-end single nucleotide A (adenine) was added. All RNA-seq libraries (non-strand-specific, paired end) were prepared with the TruSeq RNA Sample Prep kit (Illumina, USA). The 150 nt of sequence was determined from both ends of each cDNA fragment using the HiSeq platform (Illumina) according to the manufacturer. After sequencing, clean reads were obtained by removing low-quality, adaptor-polluted and high content of unknown base (N) reads. Then the clean reads were used to perform de-novo assembly with Trinity (https://github.com/trinityrnaseq/trinityrnaseq/wiki), a TGICL (http://sourceforge.net/projects/tgicl/files/tgicl%20v2.1/) was used to further assemble all the unigenes from the two different groups to form a single set of non-redundant unigenes (called all-unigenes). Sequencing reads were annotated and aligned to the *C. elegans* reference genome using Tophat2. The alignment files from TopHat2 were used to generate read counts for each gene. GO enrichment analysis was implemented by mapping each differentially expressed gene into the records of the GO database (http://www.geneontology.org/). GO terms with corrected p-values less than 0.05 were considered to be significantly enriched by differentially expressed genes. Pathway enrichment analysis was based on the KEGG database. We studied the biologically complex responses of genes and obtained pathway annotation for unigenes with KEGG annotation. A Q-value ≤ 0.05 was identified as significant enrichment of a pathway among the differentially expressed genes.

Declarations

Data Analysis. All data analysis was performed using SPSS, ver20.0 (SPSS, Chicago, IL, USA). Statistical analysis between two values was compared with a paired *t*-test. Statistical analysis among three or more values was compared with one-way ANOVA with Dunnett adjustment. Statistics indicated are: *: $p < 0.05$, **: $p < 0.01$, ***: $p < 0.001$. The lack of any symbol indicates no significant difference.

Data availability. mRNA-sequencing data are available on the NCBI Sequence Read Archive (SRA) (https://www.ncbi.nlm.nih.gov/sra), under the bioproject PRJNA662857 (https://dataview.ncbi.nlm.nih.gov/object/PRJNA662857?reviewer=dnhoor4a4e7johdlqepcm0d53h).

Acknowledgement

This work was supported by the fund from National Key R&D Program of China [2017YFD0200400 to D.P.]; National Natural Science Foundation of China [31670085 to M.S. and 31770116 to D.P.]; China Postdoctoral Science Foundation [2016M602316 to S.J.]; the Natural Science Foundation of Hubei province [2018CFB529 to S.J.]; and the College Excellent Youth Science and Technology Innovation Team Project of Hubei Province [T201535 to S.J.]. We thank Professor ZhengXing Wu for providing RNAi strains (College of Life Science and Technology, Huazhong University of Science and Technology). We also thank the Caenorhabditis Genetics Center for the worm strain. Microscopic image data were acquired at the State Key Laboratory of Agricultural Microbiology Core Facility.

Author contributions

Shouyong Ju conceived the project, Shouyong Ju and Hanqiao Chen designed and performed experiments. Shaoying Wang and Jian Lin assist to performed the experiments. Shouyong Ju and Hanqiao Chen complete the writing of the manuscript. Donghai Peng and Ming Sun designed the experiments and revised the paper.

Conflict of interest
Conflict of interest

The authors declare that they have no conflict of interest.

References

1. Janeway, C. A. & Medzhitov, R. Innate immune recognition. *Annual review of immunology* **20**, 197–216 (2002).
2. Takeuchi, O. & Akira, S. Pattern recognition receptors and inflammation. *Cell* **140**, 805–820, doi:10.1016/j.cell.2010.01.022 (2010).
3. Yu, X., Feng, B., He, P. & Shan, L. From Chaos to Harmony: Responses and Signaling upon Microbial Pattern Recognition. *Annu Rev Phytopathol* **55**, 109–137, doi:10.1146/annurev-phyto-080516-035649 (2017).
4. Wang, X., Wang, Y., Antony, V., Sun, H. & Liang, G. Metabolism-Associated Molecular Patterns (MAMPs). *Trends Endocrinol Metab*, doi:10.1016/j.tem.2020.07.001 (2020).
5. Van Crombruggen, K., Jacob, F., Zhang, N. & Bachert, C. Damage-associated molecular patterns and their receptors in upper airway pathologies. *Cellular and molecular life sciences: CMLS* **70**, 4307–4321, doi:10.1007/s00018-013-1356-7 (2013).
6. Kau, A. L., Ahern, P. P., Griffin, N. W., Goodman, A. L. & Gordon, J. I. Human nutrition, the gut microbiome and the immune system. *Nature* **474**, 327–336, doi:10.1038/nature10213 (2011).
7. Bigeard, J., Colcombet, J. & Hirt, H. Signaling mechanisms in pattern-triggered immunity (PTI). *Molecular plant* **8**, 521–539, doi:10.1016/j.molp.2014.12.022 (2015).

8. Galán, J. E. & Waksman, G. Protein-Injection Machines in Bacteria. *Cell* **172**, 1306–1318, doi:10.1016/j.cell.2018.01.034 (2018).
9. Stuart, L. M., Paquette, N. & Boyer, L. Effector-triggered versus pattern-triggered immunity: how animals sense pathogens. *Nat Rev Immunol* **13**, 199–206, doi:10.1038/nri3398 (2013).
10. Pukkila-Worley, R. Surveillance Immunity: An Emerging Paradigm of Innate Defense Activation in Caenorhabditis elegans. *PLoS pathogens* **12**, e1005795, doi:10.1371/journal.ppat.1005795 (2016).
11. Dangl, J. L. & Jones, J. D. Plant pathogens and integrated defence responses to infection. *Nature* **411**, 826–833, doi:10.1038/35081161 (2001).
12. Dunbar, T. L., Yan, Z., Balla, K. M., Smelkinson, M. G. & Troemel, E. R. C. elegans detects pathogen-induced translational inhibition to activate immune signaling. *Cell Host Microbe* **11**, 375–386, doi:10.1016/j.chom.2012.02.008 (2012).
13. Dean, P. *et al.* The enteropathogenic E. coli effector EspF targets and disrupts the nucleolus by a process regulated by mitochondrial dysfunction. *PLoS pathogens* **6**, e1000961, doi:10.1371/journal.ppat.1000961 (2010).
14. Ermolaeva, M. A. *et al.* DNA damage in germ cells induces an innate immune response that triggers systemic stress resistance. *Nature* **501**, 416–420, doi:10.1038/nature12452 (2013).
15. McEwan, D. L., Kirienko, N. V. & Ausubel, F. M. Host translational inhibition by Pseudomonas aeruginosa Exotoxin A Triggers an immune response in Caenorhabditis elegans. *Cell Host Microbe* **11**, 364–374, doi:10.1016/j.chom.2012.02.007 (2012).
16. Pellegrino, M. W. *et al.* Mitochondrial UPR-regulated innate immunity provides resistance to pathogen infection. *Nature* **516**, 414–417, doi:10.1038/nature13818 (2014).
17. Liu, Y., Samuel, B. S., Breen, P. C. & Ruvkun, G. Caenorhabditis elegans pathways that surveil and defend mitochondria. *Nature* **508**, 406–410, doi:10.1038/nature13204 (2014).
18. Melo, J. A. & Ruvkun, G. Inactivation of conserved C. elegans genes engages pathogen- and xenobiotic-associated defenses. *Cell* **149**, 452–466, doi:10.1016/j.cell.2012.02.050 (2012).
19. Galmiche, A. & Rassow, J. Targeting of Helicobacter pylori VacA to mitochondria. *Gut Microbes* **1**, 392–395, doi:10.4161/gmic.1.6.13894 (2010).
20. Cohen, T. S. *et al.* S. aureus Evades Macrophage Killing through NLRP3-Dependent Effects on Mitochondrial Trafficking. *Cell Rep* **22**, 2431–2441, doi:10.1016/j.celrep.2018.02.027 (2018).
21. Genestier, A. L. *et al.* Staphylococcus aureus Panton-Valentine leukocidin directly targets mitochondria and induces Bax-independent apoptosis of human neutrophils. *The Journal of clinical investigation* **115**, 3117–3127, doi:10.1172/jci22684 (2005).
22. Liu, Y., Samuel, B. S., Breen, P. C. & Ruvkun, G. Caenorhabditis elegans pathways that surveil and defend mitochondria. *Nature* **508**, 406–410, doi:10.1038/nature13204 (2014).
23. Pellegrino, M. W. *et al.* Mitochondrial UPR-regulated innate immunity provides resistance to pathogen infection. *Nature* **516**, 414–417, doi:10.1038/nature13818 (2014).

24. Roger, A. J., Muñoz-Gómez, S. A. & Kamikawa, R. The Origin and Diversification of Mitochondria. *Current biology: CB* **27**, R1177-r1192, doi:10.1016/j.cub.2017.09.015 (2017).
25. Monlun, M., Hyernard, C., Blanco, P., Lartigue, L. & Faustin, B. Mitochondria as Molecular Platforms Integrating Multiple Innate Immune Signalings. *J Mol Biol* **429**, 1–13, doi:10.1016/j.jmb.2016.10.028 (2017).
26. Picard, M., McEwen, B. S., Epel, E. S. & Sandi, C. An energetic view of stress: Focus on mitochondria. *Front Neuroendocrinol* **49**, 72–85, doi:10.1016/j.yfrne.2018.01.001 (2018).
27. Youle, R. J. & van der Bliek, A. M. Mitochondrial fission, fusion, and stress. *Science* **337**, 1062–1065, doi:10.1126/science.1219855 (2012).
28. Cohen, L. B. & Troemel, E. R. Microbial pathogenesis and host defense in the nematode C. elegans. *Current opinion in microbiology* **23**, 94–101, doi:10.1016/j.mib.2014.11.009 (2015).
29. Ruan, L., Crickmore, N., Peng, D. & Sun, M. Are nematodes a missing link in the confounded ecology of the entomopathogen Bacillus thuringiensis? *Trends in microbiology* **23**, 341–346, doi:10.1016/j.tim.2015.02.011 (2015).
30. Geng, C. *et al.* Dissimilar Crystal Proteins Cry5Ca1 and Cry5Da1 Synergistically Act against Meloidogyne incognita and Delay Cry5Ba-Based Nematode Resistance. *Appl. Environ. Microbiol.* **83**, doi:UNSP e03505.10.1128/AEM.03505-16 (2017).
31. Coulier, L. *et al.* Simultaneous quantitative analysis of metabolites using ion-pair liquid chromatography-electrospray ionization mass spectrometry. *Analytical chemistry* **78**, 6573–6582, doi:10.1021/ac0607616 (2006).
32. Wei, J. Z. *et al.* Bacillus thuringiensis crystal proteins that target nematodes. *Proceedings of the National Academy of Sciences of the United States of America* **100**, 2760–2765, doi:10.1073/pnas.0538072100 (2003).
33. Fang, S. *et al.* Bacillus thuringiensis bel protein enhances the toxicity of Cry1Ac protein to Helicoverpa armigera larvae by degrading insect intestinal mucin. *Applied and environmental microbiology* **75**, 5237–5243, doi:10.1128/AEM.00532-09 (2009).
34. Rambold, A. S. & Pearce, E. L. Mitochondrial Dynamics at the Interface of Immune Cell Metabolism and Function. *Trends Immunol* **39**, 6–18, doi:10.1016/j.it.2017.08.006 (2018).
35. Cogliati, S. *et al.* Mitochondrial Cristae Shape Determines Respiratory Chain Supercomplexes Assembly and Respiratory Efficiency. *Cell* **155**, 160–171, doi:10.1016/j.cell.2013.08.032 (2013).
36. Mills, E. L., Kelly, B. & O'Neill, L. A. J. Mitochondria are the powerhouses of immunity. *Nature immunology* **18**, 488–498, doi:10.1038/ni.3704 (2017).
37. Shi, J. *et al.* Systemic mitochondrial disruption is a key event in the toxicity of bacterial pore-forming toxins to Caenorhabditis elegans. *Environ Microbiol*, doi:10.1111/1462-2920.15376 (2020).
38. Liesa, M. & Shirihai, O. S. Mitochondrial dynamics in the regulation of nutrient utilization and energy expenditure. *Cell Metab* **17**, 491–506, doi:10.1016/j.cmet.2013.03.002 (2013).

39. Urano, F. *et al.* A survival pathway for Caenorhabditis elegans with a blocked unfolded protein response. *J Cell Biol* **158**, 639–646, doi:10.1083/jcb.200203086 (2002).
40. Cassidy-Stone, A. *et al.* Chemical inhibition of the mitochondrial division dynamin reveals its role in Bax/Bak-dependent mitochondrial outer membrane permeabilization. *Dev Cell* **14**, 193–204, doi:10.1016/j.devcel.2007.11.019 (2008).
41. Pardo-Lopez, L., Soberon, M. & Bravo, A. Bacillus thuringiensis insecticidal three-domain Cry toxins: mode of action, insect resistance and consequences for crop protection. *FEMS microbiology reviews* **37**, 3–22, doi:10.1111/j.1574-6976.2012.00341.x (2013).
42. Zhang, F. *et al.* Bacillus thuringiensis Crystal Protein Cry6Aa Triggers Caenorhabditis elegans Necrosis Pathway Mediated by Aspartic Protease (ASP-1). *PLoS pathogens* **12**, e1005389, doi:10.1371/journal.ppat.1005389 (2016).
43. Kho, M. F. *et al.* The Pore-Forming Protein Cry5B Elicits the Pathogenicity of Bacillus sp against Caenorhabditis elegans. *PloS one* **6**, doi:ARTN e29122.10.1371/journal.pone.0029122 (2011).
44. Griffitts, J. S. *et al.* Glycolipids as receptors for Bacillus thuringiensis crystal toxin. *Science* **307**, 922–925, doi:10.1126/science.1104444 (2005).
45. González-Juarbe, N. *et al.* Pore-forming toxin-mediated ion dysregulation leads to death receptor-independent necroptosis of lung epithelial cells during bacterial pneumonia. *Cell Death Differ* **24**, 917–928, doi:10.1038/cdd.2017.49 (2017).
46. Austin, S. & Nowikovsky, K. LETM1: Essential for Mitochondrial Biology and Cation Homeostasis? *Trends in biochemical sciences* **44**, 648–658, doi:10.1016/j.tibs.2019.04.002 (2019).
47. Lobet, E., Letesson, J. J. & Arnould, T. Mitochondria: a target for bacteria. *Biochemical pharmacology* **94**, 173–185, doi:10.1016/j.bcp.2015.02.007 (2015).
48. Fukuyama, M. *et al.* C. elegans AMPKs promote survival and arrest germline development during nutrient stress. *Biol Open* **1**, 929–936, doi:10.1242/bio.2012836.BIO2012836 (2012).
49. Brunton, J., Steele, S., Ziehr, B., Moorman, N. & Kawula, T. Feeding uninvited guests: mTOR and AMPK set the table for intracellular pathogens. *PLoS pathogens* **9**, e1003552, doi:10.1371/journal.ppat.1003552 (2013).
50. Herzig, S. & Shaw, R. J. AMPK: guardian of metabolism and mitochondrial homeostasis. *Nat Rev Mol Cell Biol* **19**, 121–135, doi:10.1038/nrm.2017.95 (2018).
51. Kristiansen, S. B. *et al.* 5-Aminoimidazole-4-carboxamide-1-beta-D-ribofuranoside increases myocardial glucose uptake during reperfusion and induces late pre-conditioning: potential role of AMP-activated protein kinase. *Basic & clinical pharmacology & toxicology* **105**, 10–16, doi:10.1111/j.1742-7843.2009.00402.x (2009).
52. Kuo, C.-J., Hansen, M. & Troemel, E. Autophagy and innate immunity: Insights from invertebrate model organisms. *Autophagy* **14**, 233–242, doi:10.1080/15548627.2017.1389824 (2018).
53. Huffman, D. L. *et al.* Mitogen-activated protein kinase pathways defend against bacterial pore-forming toxins. *Proceedings of the National Academy of Sciences of the United States of America* **101**, 10995–11000, doi:10.1073/pnas.0404073101 (2004).

54. Griffitts, J. S. & Aroian, R. V. Many roads to resistance: how invertebrates adapt to Bt toxins. *BioEssays: news and reviews in molecular, cellular and developmental biology* **27**, 614–624, doi:10.1002/bies.20239 (2005).
55. Oka, T., Toyomura, T., Honjo, K., Wada, Y. & Futai, M. Four subunit a isoforms of Caenorhabditis elegans vacuolar H+-ATPase. Cell-specific expression during development. *The Journal of biological chemistry* **276**, 33079–33085, doi:10.1074/jbc.M101652200 (2001).
56. Okkema, P. G., Harrison, S. W., Plunger, V., Aryana, A. & Fire, A. Sequence requirements for myosin gene expression and regulation in Caenorhabditis elegans. *Genetics* **135**, 385–404 (1993).
57. Nonet, M. L. *et al.* Caenorhabditis elegans rab-3 mutant synapses exhibit impaired function and are partially depleted of vesicles. *The Journal of neuroscience: the official journal of the Society for Neuroscience* **17**, 8061–8073 (1997).
58. Hardie, D. G. AMP-activated protein kinase: an energy sensor that regulates all aspects of cell function. *Genes Dev* **25**, 1895–1908, doi:10.1101/gad.17420111 (2011).
59. Greer, E. L. *et al.* An AMPK-FOXO pathway mediates longevity induced by a novel method of dietary restriction in C. elegans. *Current biology: CB* **17**, 1646–1656, doi:S0960-9822(07)01864-7.10.1016/j.cub.2007.08.047 (2007).
60. Murphy, C. T. *et al.* Genes that act downstream of DAF-16 to influence the lifespan of Caenorhabditis elegans. *Nature* **424**, 277–283, doi:10.1038/nature01789.nature01789 (2003).
61. Zečić, A. & Braeckman, B. P. DAF-16/FoxO in Caenorhabditis elegans and Its Role in Metabolic Remodeling. *Cells* **9**, doi:10.3390/cells9010109 (2020).
62. Wang, J., Nakad, R. & Schulenburg, H. Activation of the Caenorhabditis elegans FOXO family transcription factor DAF-16 by pathogenic Bacillus thuringiensis. *Developmental and comparative immunology* **37**, 193–201, doi:10.1016/j.dci.2011.08.016 (2012).
63. Chen, C. S. *et al.* WWP-1 is a novel modulator of the DAF-2 insulin-like signaling network involved in pore-forming toxin cellular defenses in Caenorhabditis elegans. *PloS one* **5**, e9494, doi:10.1371/journal.pone.0009494 (2010).
64. Hsu, A. L., Murphy, C. T. & Kenyon, C. Regulation of aging and age-related disease by DAF-16 and heat-shock factor. *Science* **300**, 1142–1145, doi:10.1126/science.1083701300/5622/1142 (2003).
65. Zhang, X. & Zhang, Y. Neural-immune communication in Caenorhabditis elegans. *Cell Host Microbe* **5**, 425–429, doi:10.1016/j.chom.2009.05.003 (2009).
66. Kanyuka, K. & Rudd, J. J. Cell surface immune receptors: the guardians of the plant's extracellular spaces. *Curr Opin Plant Biol* **50**, 1–8, doi:10.1016/j.pbi.2019.02.005 (2019).
67. Melber, A. & Haynes, C. M. UPR(mt) regulation and output: a stress response mediated by mitochondrial-nuclear communication. *Cell research* **28**, 281–295, doi:10.1038/cr.2018.16 (2018).
68. Stavru, F., Bouillaud, F., Sartori, A., Ricquier, D. & Cossart, P. Listeria monocytogenes transiently alters mitochondrial dynamics during infection. *Proceedings of the National Academy of Sciences of the United States of America* **108**, 3612–3617, doi:10.1073/pnas.1100126108 (2011).

69. Osborne, S. E. & Brumell, J. H. Listeriolysin O: from bazooka to Swiss army knife. *Philosophical transactions of the Royal Society of London. Series B, Biological sciences* **372**, doi:10.1098/rstb.2016.0222 (2017).
70. Kloft, N. *et al.* Pro-autophagic signal induction by bacterial pore-forming toxins. *Medical microbiology and immunology* **199**, 299–309, doi:10.1007/s00430-010-0163-0 (2010).
71. Carling, D., Mayer, F. V., Sanders, M. J. & Gamblin, S. J. AMP-activated protein kinase: nature's energy sensor. *Nat Chem Biol* **7**, 512–518, doi:10.1038/nchembio.610 (2011).
72. Baker, M. J. *et al.* Stress-induced OMA1 activation and autocatalytic turnover regulate OPA1-dependent mitochondrial dynamics. *EMBO J* **33**, 578–593, doi:10.1002/embj.201386474 (2014).
73. Pukkila-Worley, R. & Ausubel, F. M. Immune defense mechanisms in the Caenorhabditis elegans intestinal epithelium. *Current opinion in immunology* **24**, 3–9, doi:10.1016/j.coi.2011.10.004 (2012).
74. Li, J., Miller, E. J., Ninomiya-Tsuji, J., Russell, R. R., 3rd & Young, L. H. AMP-activated protein kinase activates p38 mitogen-activated protein kinase by increasing recruitment of p38 MAPK to TAB1 in the ischemic heart. *Circulation research* **97**, 872–879, doi:10.1161/01.RES.0000187458.77026.10 (2005).
75. Ji, W. T., Lee, L. H., Lin, F. L., Wang, L. & Liu, H. J. AMP-activated protein kinase facilitates avian reovirus to induce mitogen-activated protein kinase (MAPK) p38 and MAPK kinase 3/6 signalling that is beneficial for virus replication. *J Gen Virol* **90**, 3002–3009, doi:10.1099/vir.0.013953-0 (2009).
76. Ouimet, M. *et al.* Mycobacterium tuberculosis induces the miR-33 locus to reprogram autophagy and host lipid metabolism. *Nature immunology* **17**, 677-+, doi:10.1038/ni.3434 (2016).
77. Brenner, S. The genetics of Caenorhabditis elegans. *Genetics* **77**, 71–94 (1974).
78. Guo, S. *et al.* New strategy for isolating novel nematicidal crystal protein genes from Bacillus thuringiensis strain YBT-1518. *Applied and environmental microbiology* **74**, 6997–7001, doi:10.1128/AEM.01346-08 (2008).
79. Peng, D. *et al.* Elaboration of an electroporation protocol for large plasmids and wild-type strains of Bacillus thuringiensis. *Journal of applied microbiology* **106**, 1849–1858, doi:10.1111/j.1365-2672.2009.04151.x (2009).
80. Merritt, C. & Seydoux, G. Transgenic solutions for the germline. *WormBook: the online review of C. elegans biology*, 1–21, doi:10.1895/wormbook.1.148.1 (2010).
81. Kamath, R. S. & Ahringer, J. Genome-wide RNAi screening in Caenorhabditis elegans. *Methods* **30**, 313–321 (2003).
82. Zhang, Y., Chen, D., Smith, M. A., Zhang, B. & Pan, X. Selection of reliable reference genes in Caenorhabditis elegans for analysis of nanotoxicity. *PloS one* **7**, e31849, doi:10.1371/journal.pone.0031849PONE-D-11-22569 [pii] (2012).
83. Stocchi, V. *et al.* Simultaneous extraction and reverse-phase high-performance liquid chromatographic determination of adenine and pyridine nucleotides in human red blood cells. *Analytical biochemistry* **146**, 118–124 (1985).

84. Cortese, M. *et al.* Validation of a LC/MSMS method for simultaneous quantification of 9 nucleotides in biological matrices. *Talanta* **193**, 206–214, doi:10.1016/j.talanta.2018.10.003 (2019).
85. Wang, J. M. *et al.* Simultaneous determination of creatine phosphate, creatine and 12 nucleotides in rat heart by LC-MS/MS. *J Chromatogr B Analyt Technol Biomed Life Sci* **958**, 96–101, doi:10.1016/j.jchromb.2014.03.008 (2014).
86. Palikaras, K., Lionaki, E. & Tavernarakis, N. Coordination of mitophagy and mitochondrial biogenesis during ageing in C. elegans. *Nature* **521**, 525–528, doi:10.1038/nature14300 (2015).
87. Cristina, D., Cary, M., Lunceford, A., Clarke, C. & Kenyon, C. A regulated response to impaired respiration slows behavioral rates and increases lifespan in Caenorhabditis elegans. *PLoS genetics* **5**, e1000450, doi:10.1371/journal.pgen.1000450 (2009).
88. Lakshmanan, L. N. *et al.* Clonal expansion of mitochondrial DNA deletions is a private mechanism of aging in long-lived animals. *Aging Cell* **17**, e12814, doi:10.1111/acel.12814 (2018).
89. Fujishima, A. *et al.* Live visualisation of electrolytes during mouse embryonic development using electrolyte indicators. *PloS one* **16**, e0246337, doi:10.1371/journal.pone.0246337 (2021).
90. Luke, C. J. *et al.* An intracellular serpin regulates necrosis by inhibiting the induction and sequelae of lysosomal injury. *Cell* **130**, 1108–1119, doi:10.1016/j.cell.2007.07.013 (2007).
91. Bischof, L. J., Huffman, D. L. & Aroian, R. V. Assays for toxicity studies in C. elegans with Bt crystal proteins. *Methods in molecular biology* **351**, 139–154, doi:10.1385/1-59745-151-7:139 (2006).
92. Los, F. C., Ha, C. & Aroian, R. V. Neuronal Goalpha and CAPS Regulate Behavioral and Immune Responses to Bacterial Pore-Forming Toxins. *PloS one* **8**, e54528, doi:10.1371/journal.pone.0054528.PONE-D-12-33795 (2013).
93. Jiu, Y., Jin, C., Liu, Y., Holmberg, C. I. & Jäntti, J. Exocyst subunits Exo70 and Exo84 cooperate with small GTPases to regulate behavior and endocytic trafficking in C. elegans. *PloS one* **7**, e32077, doi:10.1371/journal.pone.0032077 (2012).

Figures

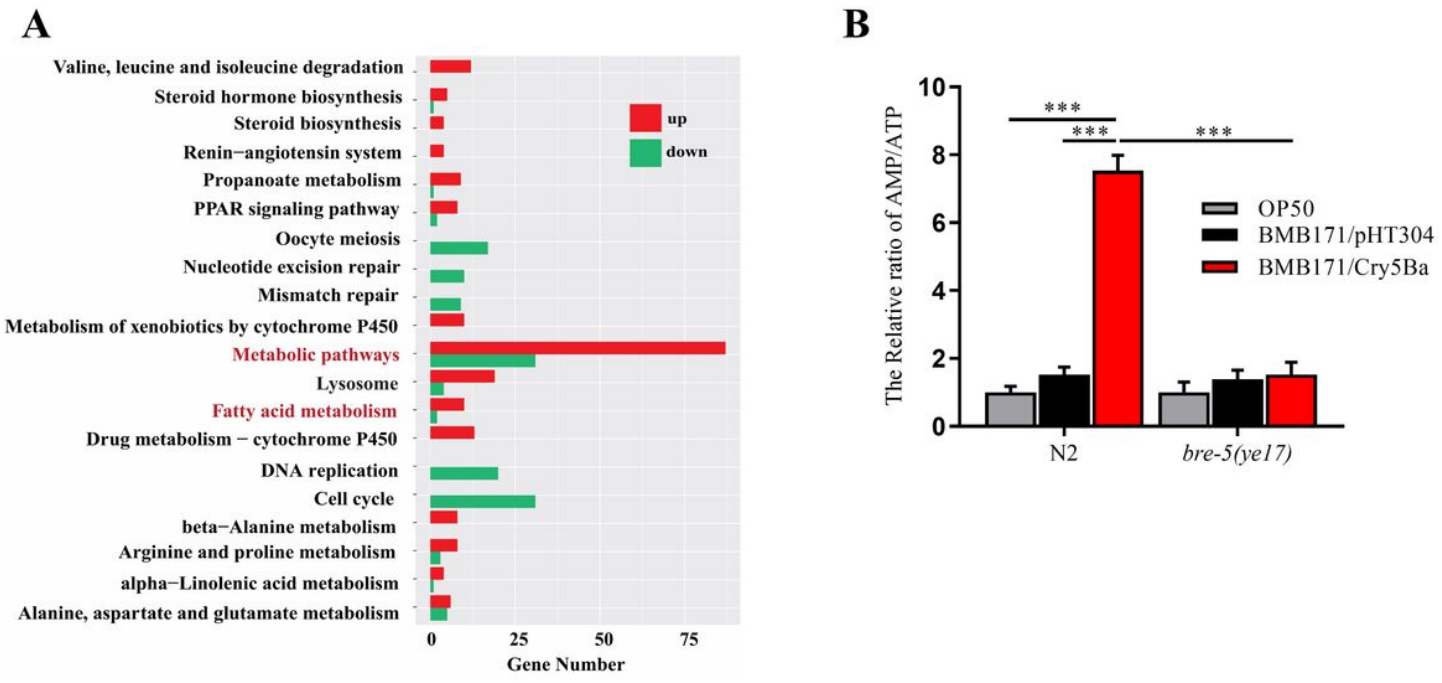

Figure 1

Nematicidal Bt infection leads to the energy imbalance in C. elegans. (A) The top 20 pathways affected by the infection of nematicidal Bt obtained by the enrichment pathway analyses of RNA-Seq data. (B) Analysis of the AMP/ATP ratio of wild-type N2 and Cry5Ba-receptor null mutant bre-5(ye17) worms fed with OP50, BMB171/pHT304 and BMB171/Cry5Ba. The mean and SD of three independent replicates are shown. Values differences were calculated by one-way ANOVA. Triple asterisks (∗∗∗) are set at p< 0.001, two asterisks (∗∗) are set at p< 0.01. a single asterisk (∗) is set at p<0.05.

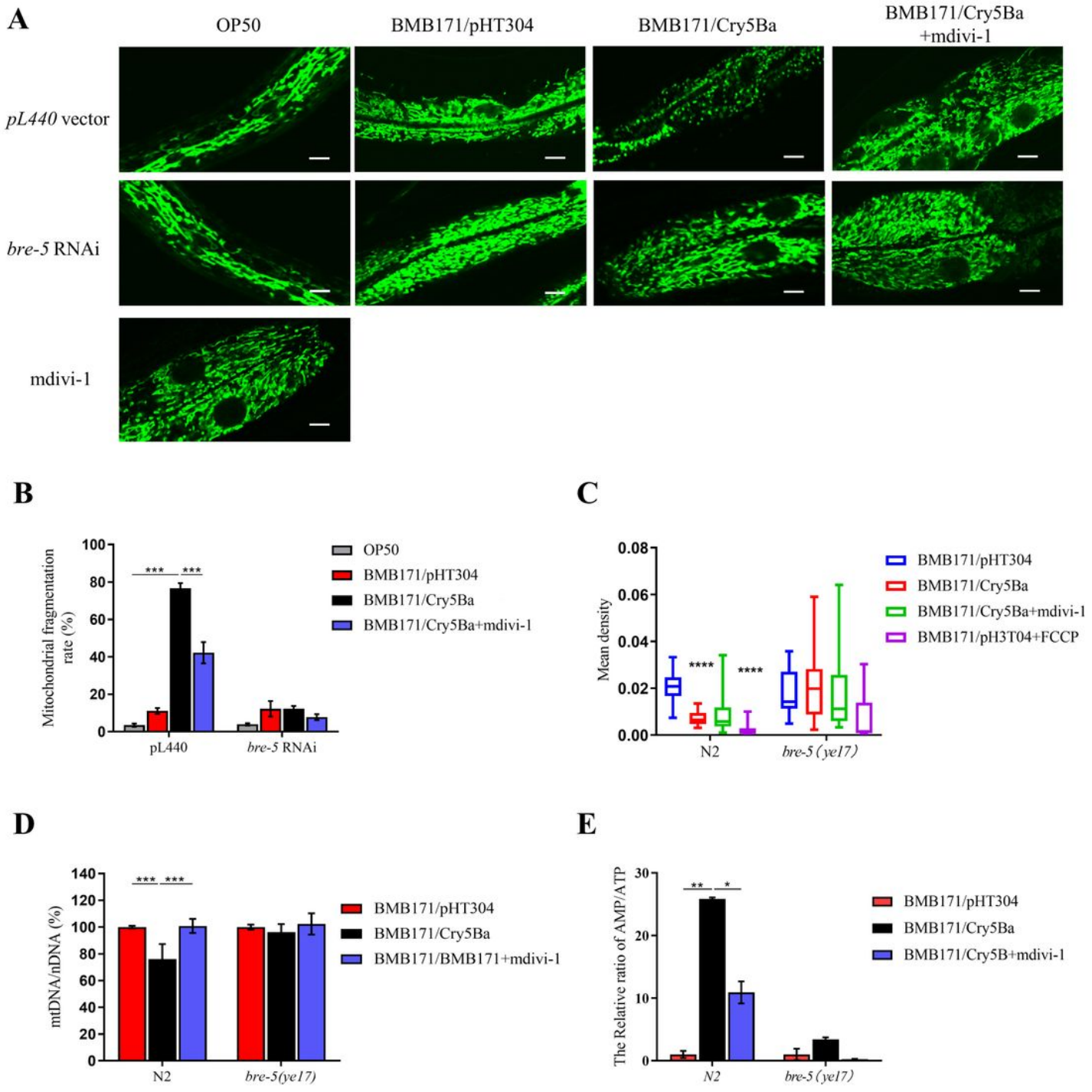

Figure 2

B. thuringiensis infection leads to mitochondria damage. (A). Observe the mitochondrial morphology of transgenic C. elegans SJ4143(zcIs17 [Pges-1::GFPmt]), which were fed with different bacteria under bre-5 RNAi or not. The representative images of worms treated by each strain are shown. The scan bars represent 20 μm. (B) Analysis of the percentage of worms that showed MF phenotype after treatment with each Bt strain. Transgenic worms subjected to bre-5 RNAi or empty vector were treated with different

strains.. (C) Analysis of the mitochondrial membrane potential (ΔΨm)) under each treatment. The level of ΔΨm was determined by densitometry of each worm. Around 20 worms were measured in each condition. (D) The relative ratio of mtDNA /nDNA was investigated by Real-time PCR and then analyzed. (E) The relative AMP/ATP ratio was measured in each condition. In each assay, the mean and SD of three independent replicates are shown. Values differences were calculated by one-way ANOVA. Triple asterisks (∗∗∗) are set at p< 0.001, two asterisks (∗∗) are set at p< 0.01. a single asterisk (∗) is set at p<0.05.

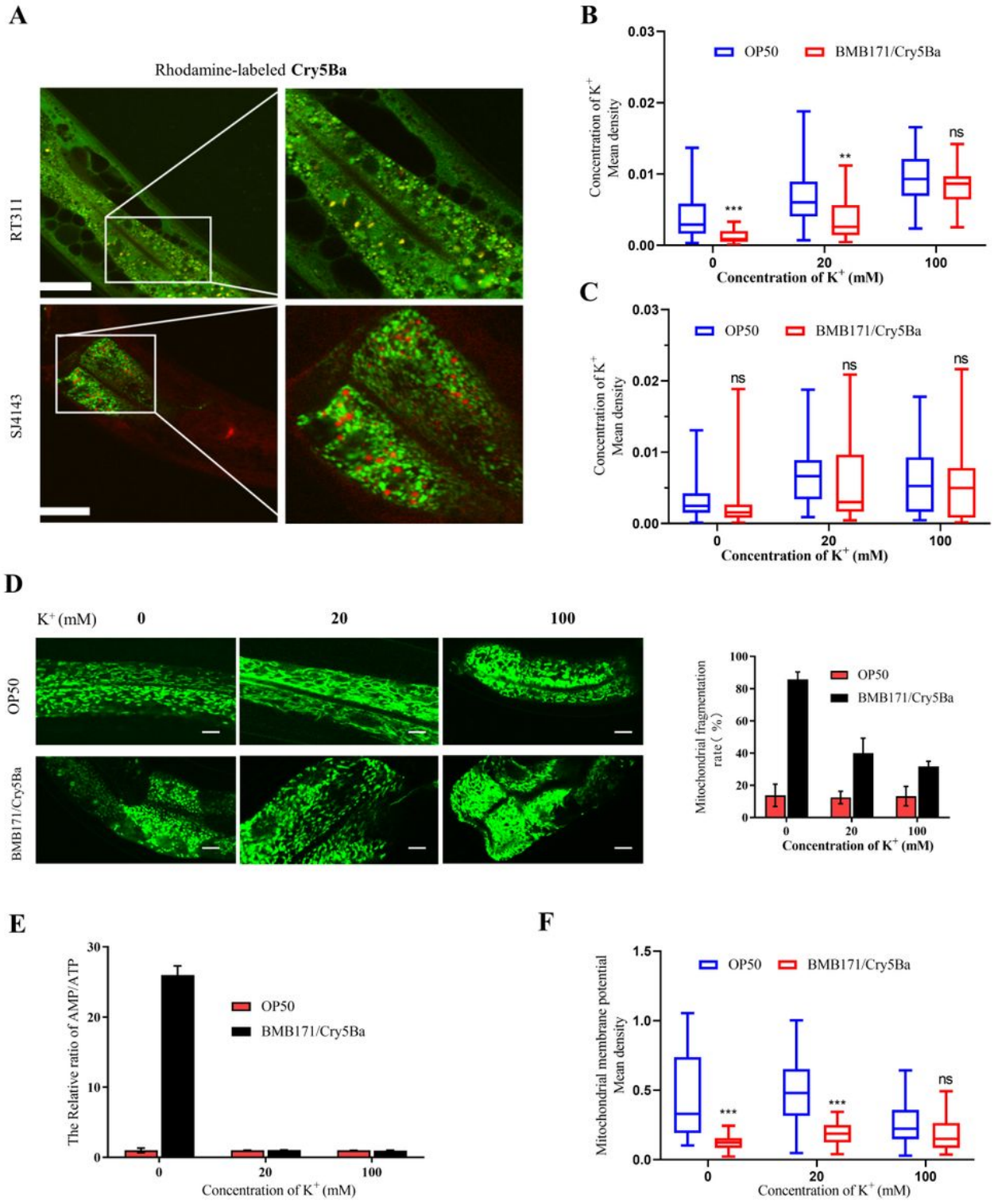

Figure 3

Intracellular potassium leakage caused mitochondrial damage in C. elegans. (A) The fluorescent confocal micrograph of transgene worm RT311[Pvha-6::GFP::RAB-11] and SJ4143(zcIs17 [Pges-1::GFPmt]) that fed by the Rhodamine-labeled Cry5Ba protein.. Scale bar is 10 μm. (B) and (C) Under different potassium environments, quantitatively detect the intracellular potassium concentration during C. elegans N2 (B) and bre-5 (C) treated by Cry5Ba/BMB171. At least 20 worms need to be measured in each condition. (D) C. elegans SJ4143(zcIs17 [Pges-1::GFPmt]) were used to visualize the mitochondrial morphology, which was fed with OP50 or Cry5Ba/BMB171 under different potassium environment. The representative images of worms treated by each strain are shown. The chart shows the proportion of worms that showed MF phenotype in each condition. The scan bars represent 20 μm. (E) Analysis of the mitochondrial membrane potential (ΔΨm)) under Cry5Ba/BMB171 treatment in each condition. At least 20 worms need to be measured. (F) The relative AMP/ATP ratio is measured in different potassium environments with Cry5Ba/BMB171 treatment or not. Values differences were calculated by one-way ANOVA. Triple asterisks (∗∗∗) are set at $p < 0.001$, two asterisks (∗∗) are set at $p < 0.01$.ns showed no significance criteria.

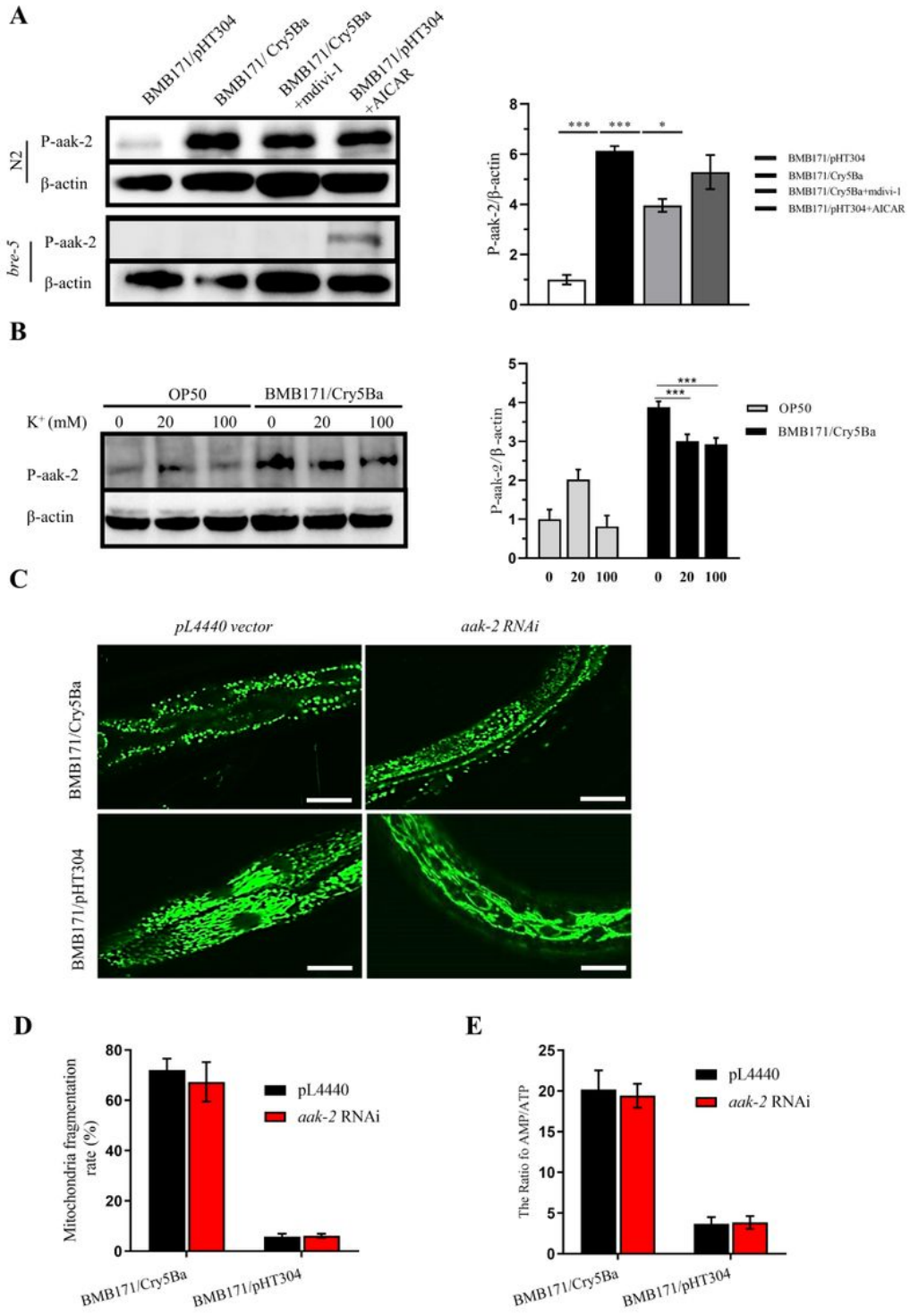

Figure 4

AMPK was induced by nematicidal Bt infection. (A) Left: western blotting showed that AMPK was activated by the phosphorylation of the protein AAK-2 when exposed to BMB171/Cry5Ba after 4 h. Right: amounts of p-AAK-2 were determined by densitometry of protein bands from three independent experiments. β-actin was the loading control. (B) left: The western blot results showed the phosphorylation of the protein AAK-2 when exposed to BMB171/Cry5Ba in different potassium

environments. Right: the chart showed the quantitative results of the phosphorylation level of AAK-2 relative to the concentration of β-actin. In each assay, the mean and SD of three independent replicates are shown. (C) The mitochondria morphologies observations of transgenic C. elegans SJ4143(zcIs17[Pges-1::GFPmt]) fed with BMB171/Cry5Ba or BMB171/pHT304. Representative images of worms treated by each strain are shown. The scan bars represent 20 μm. (D) After aak-2 RNAi, analysis of the percentage of worms showing MF phenotype after treatment with BMB171/PHT304 and BMB171/Cry5Ba. (E) Analysis of the AMP/ATP ratio after treated by BMB171/pHT304 and BMB171/Cry5Ba when aak-2 RNAi. In each condition, the mean and SD of three independent replicates are shown. Values differences were calculated by one-way ANOVA. Triple asterisks (∗∗∗) are set at p< 0.001, a single asterisk (∗) is set at p<0.05.

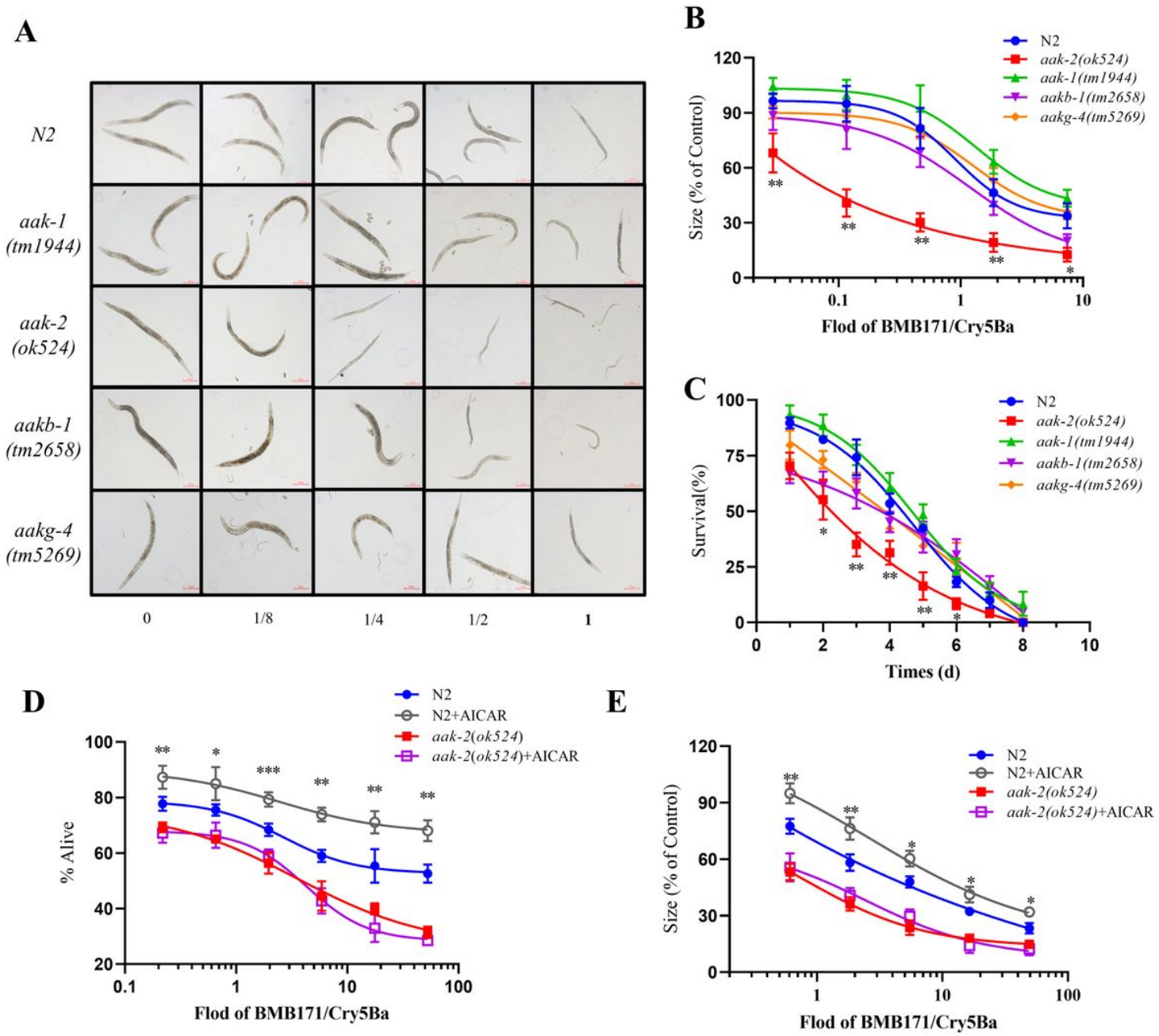

Figure 5

The AMPK activation is involved in C. elegans defense responses against Bt infection (A) The growth assay of the wild type N2 and mutant worms after BMB171/Cry5Ba infection. The representative worms are shown for each dose. Scale bar, 0.02 mm. (B) To photographed at least 60 worms for each dose under 100 magnification microscope, calculated the average area for each condition. The size of the worms in the absence of toxin was set at 100%. (C) The survival assay of the wild type worms N2 and mutant worms after BMB171/Cry5Ba infection. The survival assay (D) and the growth assay (E) of the wild type worms N2 and mutant worms aak-2(ok524) after BMB171/Cry5Ba infection when the AMPK was activated by AICAR or not. The mean and SD of three independent replicates are shown. Asterisks indicate significance as determined by a Student's t-test (*, $p<0.05$; **, $p<0.01$) and ns indicate no significant difference.

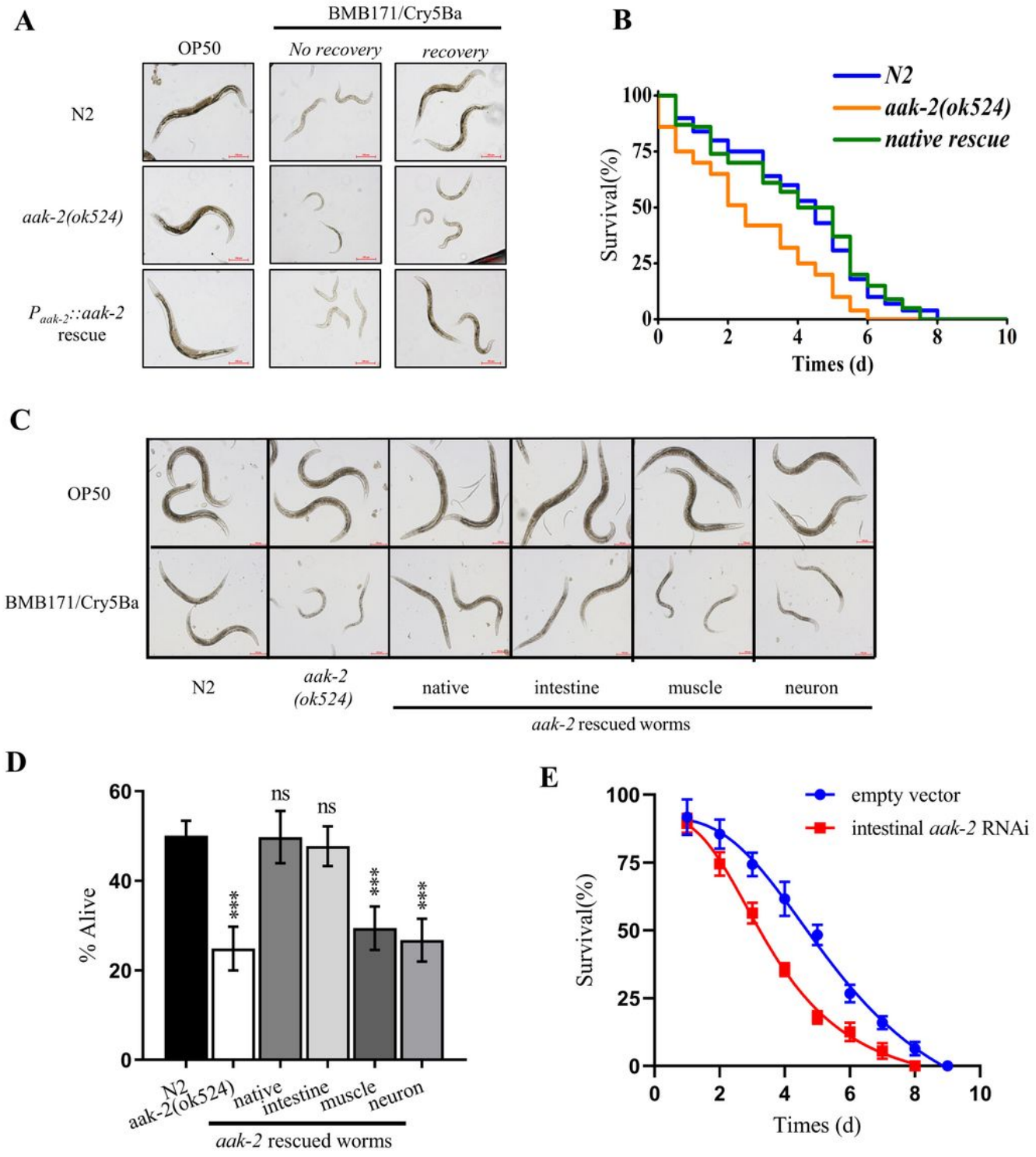

Figure 6

AMPK activity in the intestine is required for C. elegans resistance to Bt infection. (A) The growth assay of the C. elegans N2, aak-2(ok524) and Paak-2::aak-2 rescue worms after fed with OP50 or BMB171/Cry5Ba for 30 min and then recovery in E. coli OP50 NGM plate for 24h or not. The representative images of worms in each condition are shown. (B) The survival assay of the C. elegans N2, aak-2(ok524) and Paak-2::aak-2 rescue worms after treated by BMB171/Cry5Ba. (C) The growth assay of the C. elegans N2, aak-

2(ok524) and several kinds of rescue worms after fed with OP50 or BMB171/Cry5Ba. The representative images of worms in each condition are shown. (D) The survival assay of the wild type worms N2, aak-2(ok524) and several kinds of rescue worms after BMB171/Cry5Ba infection. (E) The survival assay of the N2 worms after BMB171/Cry5Ba infection when intestinal aak-2 RNAi or not. The mean and SD of three independent replicates are shown. Values differences were calculated by one-way ANOVA. Triple asterisks (***) are set at p< 0.001 and ns indicates no significant difference.

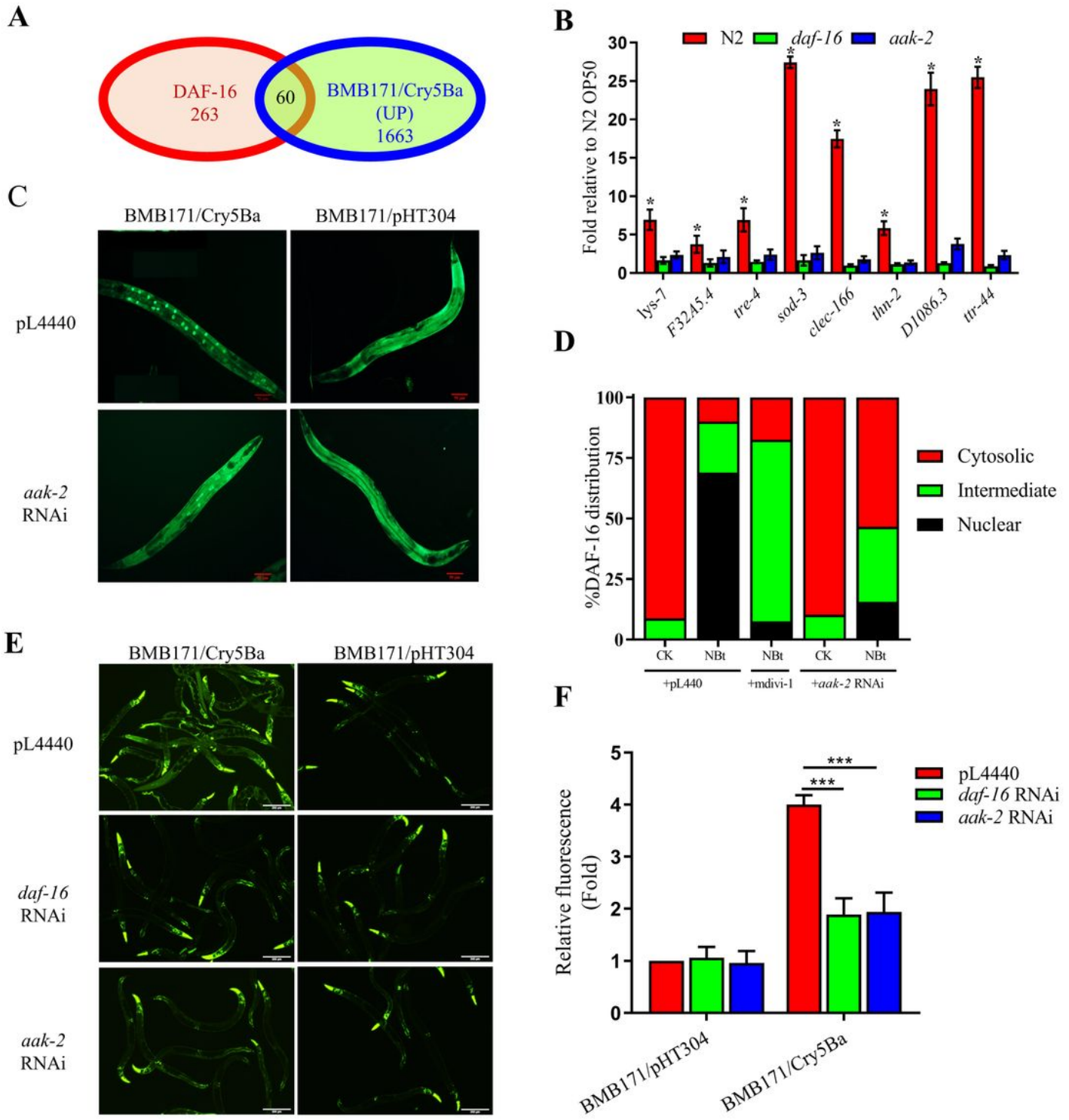

Figure 7

AMPK is required for DAF-16 nuclear accumulation during Bt infection. (A) Venn diagrams comparing show the overlaps in genes activated by nematicidal Bt and the target genes of DAF-16 in C. elegans. (B) qPCR analysis of expression of DAF-16 target genes in wild-type N2, aak-2(ok524) and daf-16(mu861) mutant worms after Bt infection. (C) DAF-16 translocation was observed during the no-RNAi and aak-2 RNAi transgenic worms TJ356(Isdaf-16::gfp) fed with BMB171/Cry5Ba or BMB171/pHT304 for 2 h, respectively. The representative images for each treatment are shown. Scale bar, 20 μm. (D) The quantification of DAF-16 distribution after Bt infection (CK: BMB171/pHT304; NBt: BMB171/Cry5Ba). The worms with DAF-16 locations as cytosolic (Cyt), intermediate (Int), or nuclear (Nuc) were counted, and the percentages of each pattern of DAF-16 nuclear translocation are calculated. (E) The expression level of Psod::GFP were observed using a reporter strain CF1553 (Psod::GFP) during the aak-2 RNAi, daf-16 RNAi or not after Bt infection. Scale bar, 20 μm. (F) The quantification of Psod::GFP expression levels calculated by the fluorescence intensity. The mean and SD of three independent replicates are shown. Values differences were calculated by one-way ANOVA. Triple asterisks (∗∗∗) are set at $p < 0.001$, two asterisks (∗∗) are set at $p < 0.01$, one asterisk was set at $p < 0.05$ and ns indicate no significant difference.

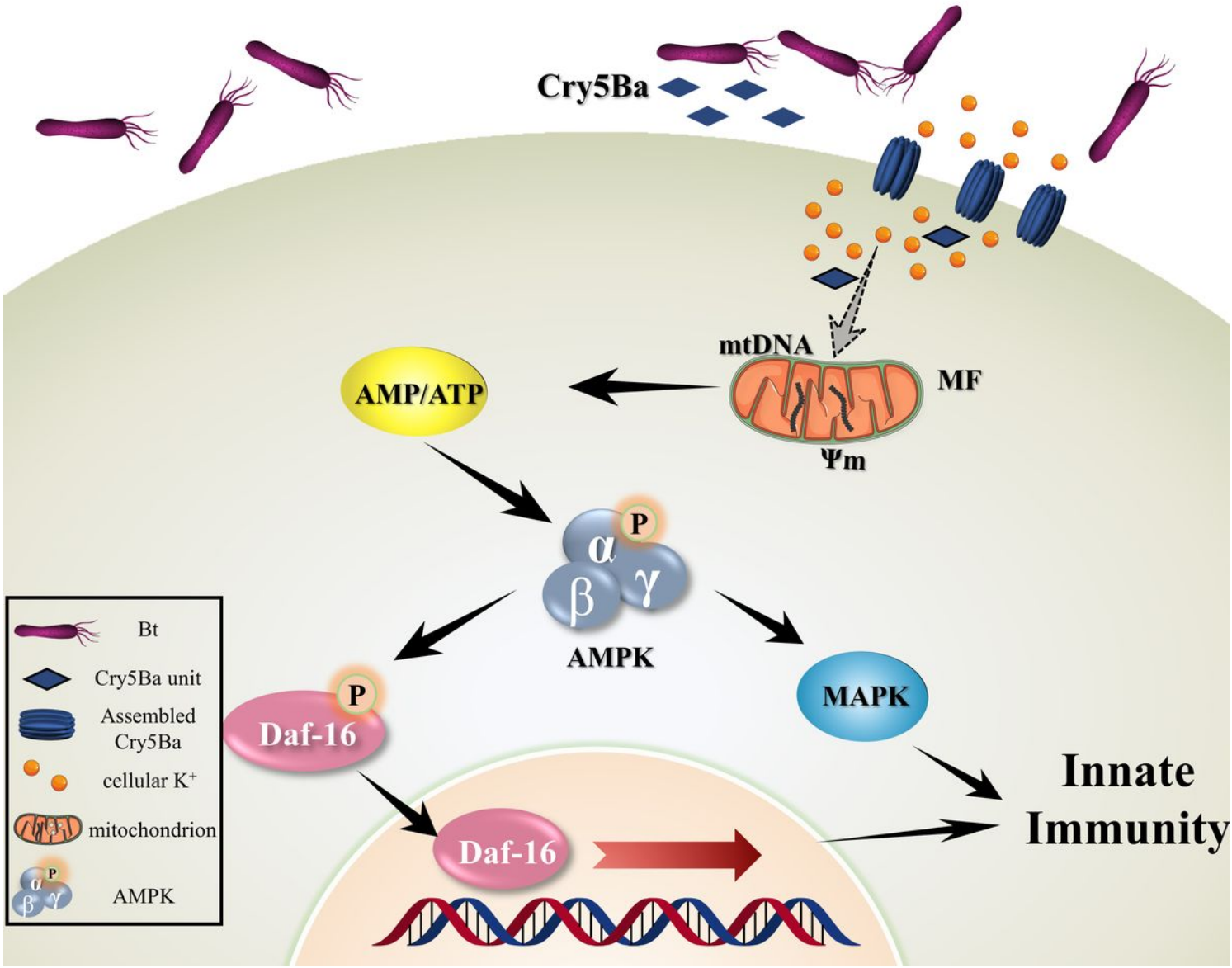

Figure 8

The action model of mitochondria surveillance systems recognition the pathogens and activation innate immune responses by AMPK in C. elegans. After nematicidal Bt spores and crystals mixture was fed to the worms, the Cry5Ba toxin assembled to trigger pore formation and transport into the intestinal epithelial cells of C. elegans, and disrupts mitochondria indirectly that lead to MF, a decrease in mitochondrial membrane potential, and the changes in mtDNA content, resulting in intercellular energy imbalance. The AMPK senses Bt-caused intercellular ATP changing and activated the AMPK by phosphorylating AAK-2. The activated AAK-2 modulates conversationally DAF-16-dependent and p38-MAPK dependent innate immune pathways to defense pathogens. Solid arrows represent relationship has been confirmed in this study. The dotted arrow represents the relationship is still unclear.

Supplementary Files

This is a list of supplementary files associated with this preprint. Click to download.

- SupplementalTableS1.xlsx
- SupplementalTableS2.xlsx
- SupplementalTableS3.xlsx
- Supplementalinformation.docx